QUADRATURE RADAR DEMODULATION TECHNIQUES

FOR ACCURATE DISPLACEMENT DETECTION

A DISERTATION SUBMITTED TO THE GRADUATE DIVISION OF THE UNIVERSITY OF HAWAIʻI AT MĀNOA IN PARTIAL FULFILLMENT OF THE REQUIREMENTS FOR THE DEGREE OF

DOCTOR OF PHILOSOPHY

IN

ELECTRICAL ENGINEERING

BY

SHUHEI YAMADA

OCTOBER 2016

Thesis Committee:

Victor M. Lubecke, Chairperson

Olga Boric-Lubecke

Zhengqing Yun

David Garmire

Jelena Maricic

Acknowledgements

I would like to express my sincere appreciation to my advisor Professor Victor Lubecke, and Professor Olga Boric-Lubecke for their great support and advice for this study. Without them, I could not complete this dissertation and achieve this goal. I also would like to express my sincere gratitude to Professor Maricic, Professor Garmire, and Professor Yun for serving on my dissertation committee. I also would like to express my gratitude to my family for their sincere support, with special thanks to my parents for their help to study and live abroad. I also would like to express my sincere gratitude to Andrea Yuen and her family for their great support and for treating me like a member of their family. Finally, I would like to thank all of my friends for their sincere support in my day-to-day life.

Abstract

Microwave Doppler radar systems can be used to measure human vital signs by tracking torso displacement. Technical requirements for such systems depend on detection object and objective, resolution and sensitivity, as well as practical constraints such as cost, size and power consumption. Due to its simple structure and validity, direct conversion systems are commonly used for vital signs detection applications. One problem with such systems is that motion or displacement detection accuracy is often compromised by the presence of dc offset that limits the overall signal to noise ratio (SNR) and the system resolution. While the portion of dc offset caused by system imperfections and the external environment is problematic, the dc offset contributed from the subject is critical for accurate displacement measurement. In this research, dc offset optimization methods for direct conversion systems are studied. A method is proposed to make possible accurate measurements of a moving subject, through a system which preserves useful dc contributions while eliminating non-essential dc components which would otherwise undermine the use of appropriate gain and resolution. The performance is contrasted with an ac coupling method using high-pass or band-pass filters and other established dc management approaches.

Table of Contents

Table of figures

CHAPTER 1

RESEARCH BACKGROUND

1.1 Introduction

Microwave Doppler radar systems can be used to measure human vital signs by tracking torso displacement. There are a wide variety of applications of this technology such as medical, disaster rescue, security, and occupancy sensing [1-2]. System requirements for such radar systems depend on the detection object and objective, resolution and sensitivity, as well as practical constraints such as cost, size and power consumption [3]. Due to its simple structure and validity, one of the most commonly used systems is the quadrature direct conversion system. It consists of a local oscillator that generates the RF carrier signal and a mixer that converts the modulated RF signal to a baseband signal. In addition, the system has two output signals for the sake of image rejection by creating the two orthogonal signals. Since this system has two output signals, one of the signals is called the in-phase signal, and the other is called the quadrature phase signal. Thus, such system is called a quadrature direct conversion system. Due to its two output signals, this system requires the phase demodulation processes in order to obtain the phase variation information caused by the motion of the subject. For signal processing, there are two major methods. One is linear demodulation, and the second is non-linear demodulation. Linear demodulation is based on the property of the eigenvector and the covariance matrix; sometimes it is called eigenvector demodulation. On the other hand, non-linear demodulation is based on the property of arctangent function; therefore

it is sometimes called arctangent demodulation. These two demodulation methods have different advantages and disadvantages, as well as detection limitations and hardware constraints.

1.2 Issues in Accurate Displacement Detection

1.2.1 Hardware Issues

Fig. 1 shows the block diagrams of the direct conversion systems ((a) Receiver, (b) Transceiver). Due to the finite mixer port-to-port isolation, the LO signal can leak through the mixer RF port. To drive a mixer properly while obtaining low conversion loss, typically a high LO power is required, which may result in significant LO leakage from the RF port. The LO leakage from the RF port of the Mixer in the receiver configuration is separated into two components. One is external LO leakage, which affects other receivers, and the other is an LO self-mixing signal which induces dc offset and harmonics. In addition to leakage problems in bistatic configuration, in a monostatic configuration (b), there is transmitting chain (Tx) signal leakage to the receiver chain (Rx), which results in a self-mixing component. The LO leakage can also be radiated by the antenna as “external LO leakage”, and may affect the transmitted signal as well as the operation of other receivers. The LO leakage to the receiver chain is also reflected by other components such as the LNA and antenna, and can thus get back to the mixer causing the LO self-mixing which generates the second harmonic ($2f_{LO}$) components and the dc offset. Although the harmonics can be rejected by a LPF or BPF, the dc offset will be directed to the baseband signal processing IC, and may result in measurement error. While the dc offset can be cancelled at the output of the mixer with significantly

increasing the complexity of baseband system [4-5].

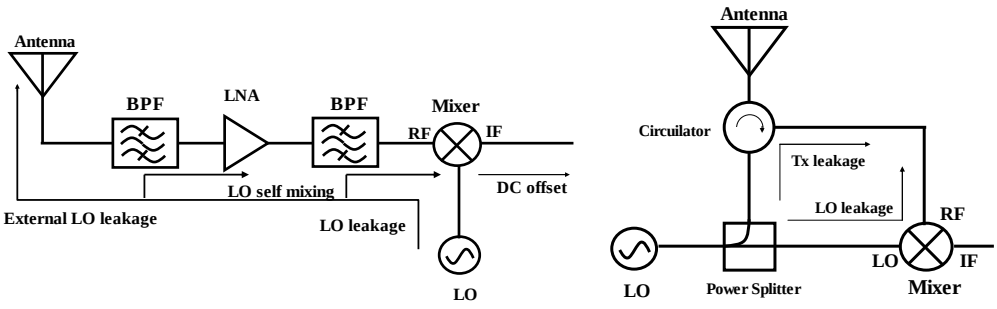

(a) Receiver (b) Transceiver

Fig. 1 Block diagram of direct conversion systems

1.2.2 Signal Processing Issues

Assuming that the target's time varying motion is given by $\Delta x(t)$, the quadrature baseband output assuming balanced channels can be expressed as:

$$B(t) = A_r \exp\left[\theta + 4\pi \Delta x(t)/\lambda\right] \quad \text{(Eq. 1.1)}$$

where θ is the constant phase shift related to the phase change at the surface of a subject and the phase delay between the mixer and antenna. Applying arctangent demodulation to the ratio of the quadrature outputs, phase information linearly proportional to target' s motion can be extracted as:

$$f(t) = \arctan\left(\frac{B_Q(t)}{B_I(t)}\right) = \arctan\left(\frac{A_r \sin(\theta + p(t))}{A_r \cos(\theta + p(t))}\right) \quad \text{(Eq. 1.2)}$$

where $p(t) = 4\pi\Delta x(t)/\lambda$ is the superposition of the phase information due to the motion of the target. However, dc offsets in quadrature channels act as a linear transform on the I and Q components; the quadrature baseband output assuming balances channels can be

expressed as:

$$B'(t) = V_r + A_r \exp\left[\theta + 4\pi\Delta x(t)/\lambda\right] \quad \text{(Eq. 1.3)}$$

where V_r is the dc offset caused by imperfection of the system and external environment. Thus, the arctangent demodulation output becomes:

$$\phi'(t) = \arctan\left(\frac{B'_Q(t)}{B'_I(t)}\right) = \arctan\left(\frac{V_Q + A_r \sin(\theta + p(t))}{V_I + A_r \cos(\theta + p(t))}\right) \quad \text{(Eq. 1.4)}$$

where V_I and V_Q refer to the dc offsets of each channel [6]. This dc signal contains the dc offset caused by the imperfection of the direct conversion system explained previously, as well as the dc offset caused by the external environment. In order to achieve accurate demodulated signals, it is important to take into account and distinguish the unwanted dc offset.

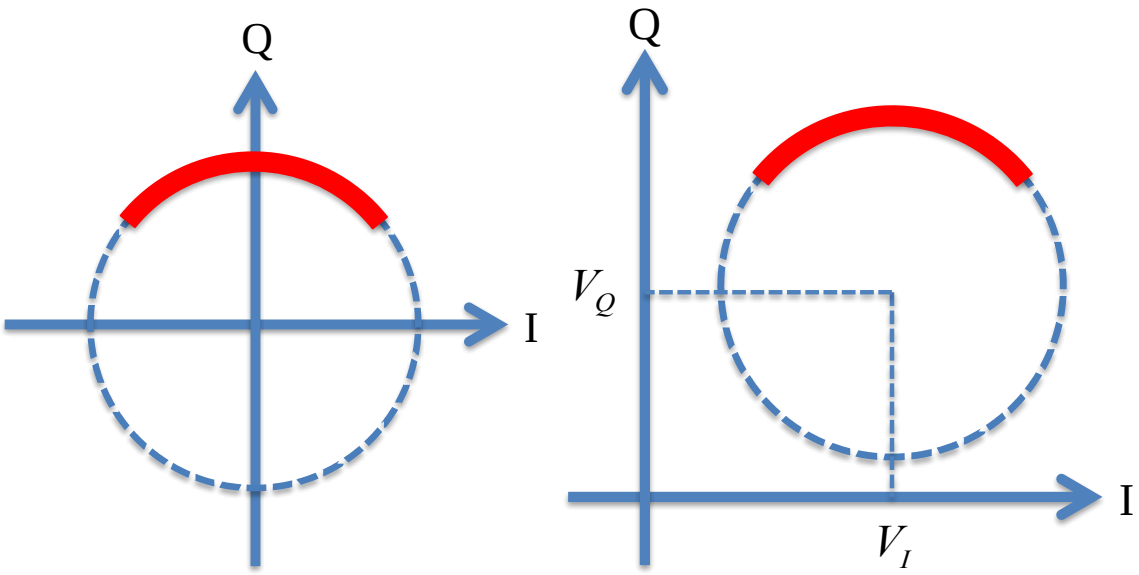

(a) Without dc offset (b) With dc offset

Fig. 2 Arc with and without dc offset

1.3 Existing Methods

1.3.1 AC coupling

The conventional method to remove the dc offset is filtering. The unwanted dc offset can be removed by implementing either a high-pass filter or a band-pass filter, and only signal can pass through. Such a filter is usually implemented at the first stage of the baseband system so that it removes the unwanted dc offset before the amplifications to avoid the saturation. Due to its simplicity and effectiveness, this method is most commonly used with the direct conversion system. However, this method has some disadvantages. For biomedical applications, the frequency of acquired signals is very low. Thus the cut-off frequency of the filter has to be lower than the signal frequency. In order to create such low cut-off frequency, a large value of capacitor and resister are required. This is usually about several microfarad of capacitor and mega-ohm of resistor. Such large values of capacitor and resistor result in a large time constant, which significantly affects the dc settling time. Such a degraded transient response affects the signal integrity. In Fig. 3, the IQ signal of AC coupled direct conversion system is shown. Due to the increased dc settling time, the output signal is distorted and therefore it does not create a clear arc shape on complex IQ plot.

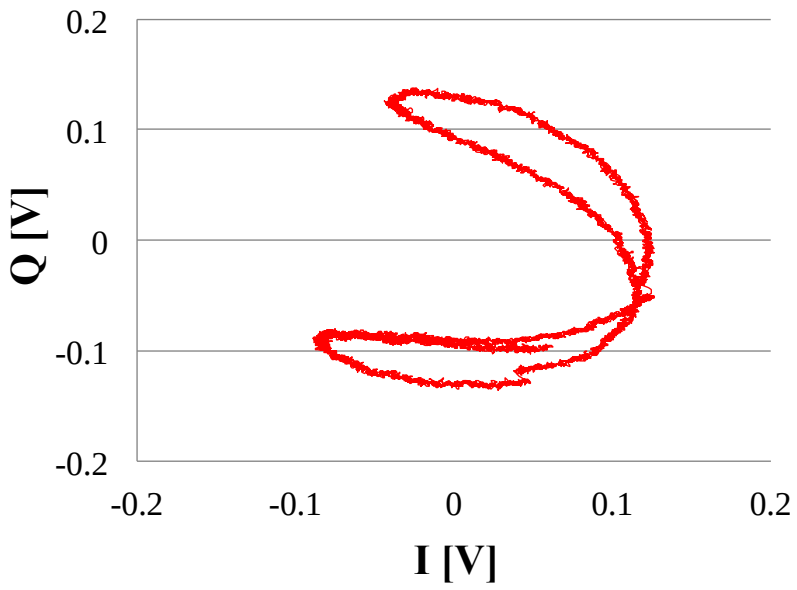

Fig. 3 IQ plot of ac coupled system

1.3.2 DC offset compensation

Another method to remove the dc offset is cancelling by a differential amplifier. This can be done by manually or digitally adjusting the supply voltage of one input of a differential amplifier [4-5]. In Fig. 4, the dc offset compensation architectures are shown. Both systems work as no dc offset after the calibration is done precisely. However, it requires hardware modifications and significant signal processing to achieve the desired signal. Especially for the digitally controlled method, since it involves a feedback system, it always contains some time delay until it compensates the dc offset. In Fig. 5, the dc offset of the digital compensation method is shown. It requires more than 30 seconds to set the dc offset level precisely. Thus, this method requires a huge measurement delay.

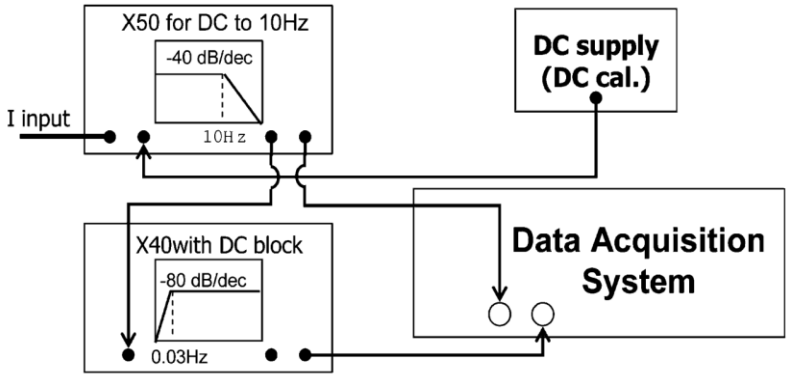

(a) Manual dc offset compensation

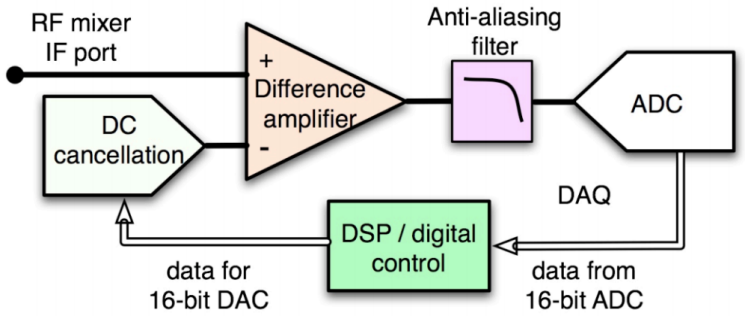

(b) Digital dc offset compensation

Fig. 4 DC offset compensation Architectures

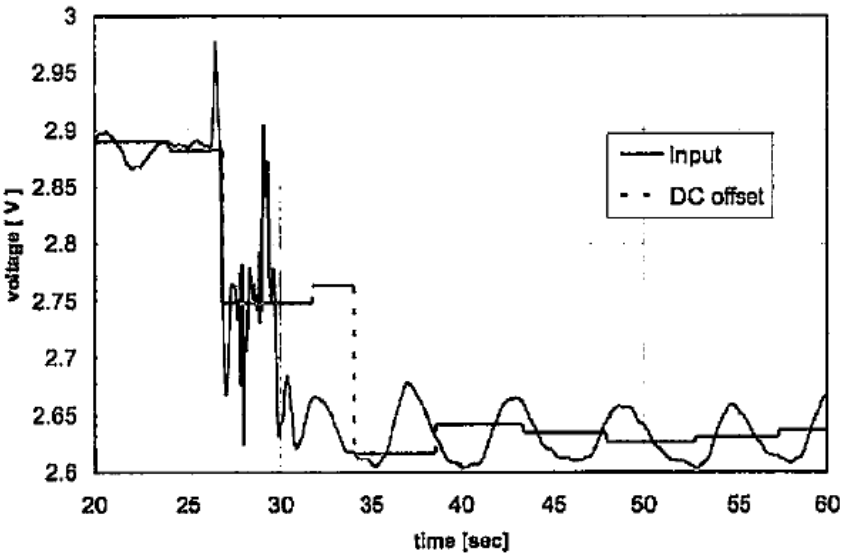

Fig. 5 Digital dc offset compensation

1.3.3 Minimum gain dc coupling method

Another method is acquiring all the dc components without filtering out with minimum gain of baseband amplifier, as shown in Fig. 6. This method overcomes the problem caused by the ac coupling method. However it creates other drawbacks. The dc offset is typically several orders of magnitude larger than the periodic signal related to human cardio activities. This method simply sacrifices the dynamic range and resolution of ADC. In addition, the minimum amount of gain reduces the signal to noise ratio as shown in Fig. 7, which degrades the radar sensitivity significantly.

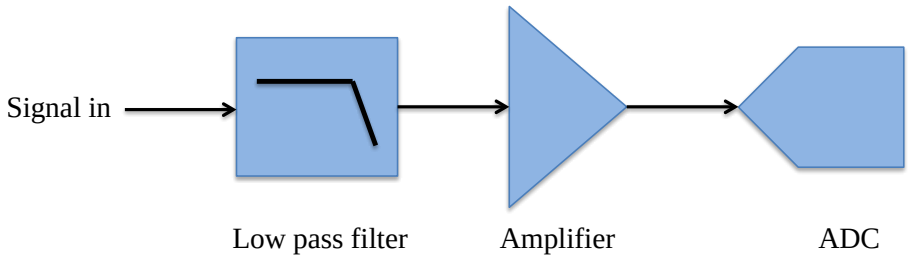

Fig. 6 Minimum gain dc coupling system block diagram

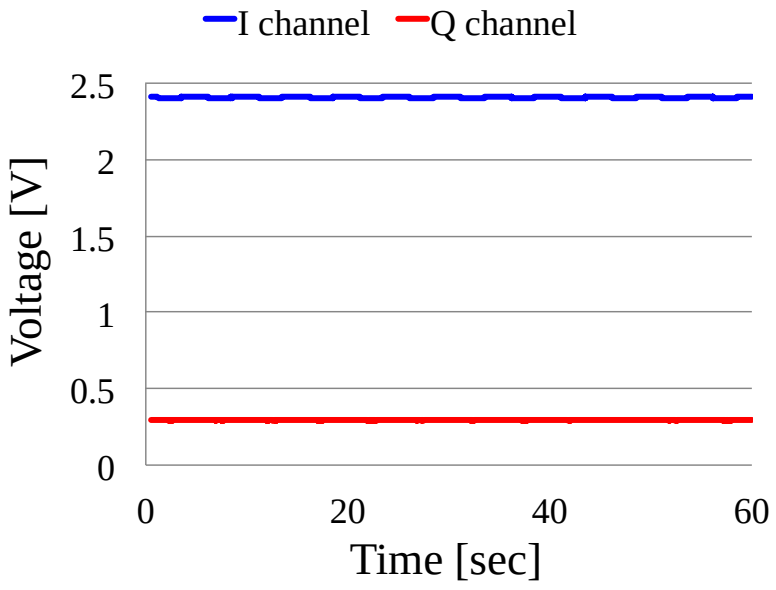

Fig. 7 Acquired data

1.3.4 Low-IF architecture

The Low-IF architecture shown in Fig. 8 is a type of a heterodyne system in which the IF signal frequency is low enough so that it can be digitized directly with an ADC [7]. Since this system does not convert the RF to baseband signal, low-IF system outputs can be ac coupled without suffering the dc settling issue. The clutter reflections and leakage will result in a signal at low-IF frequency, which can be easily removed from the wanted signal in the digital domain. Another advantage of this system is the low noise floor level. Since it avoids the signal falls into the frequency band which the flicker noise is the dominant noise floor. Thus, it can achieve better SNR, which results in better sensitivity. In addition, low-IF architecture requires only one receiver chain for full phase recovery, resulting in simpler architecture that is more amenable to array implementation. Due to those advantages, this system is commonly used in a number of wireless communication systems. However, this system architecture requires complex hardware, faster sampling rate, intense signal processing, image rejection, and high power consumption. For human vital signs detection, the frequency of such motion is usually around 1Hz, or even less. However, with the low-IF system, the sampling rate needs to be high enough that usually kHz to MHz to capitalize on the advantages described above. Therefore, this system needs significantly over sampling. It also requires image rejection since the mixer generates $LO + RF$ and $LO - RF$ signals that only kHz to MHz apart. Therefore the requirement for such image rejection filter becomes more stringent.

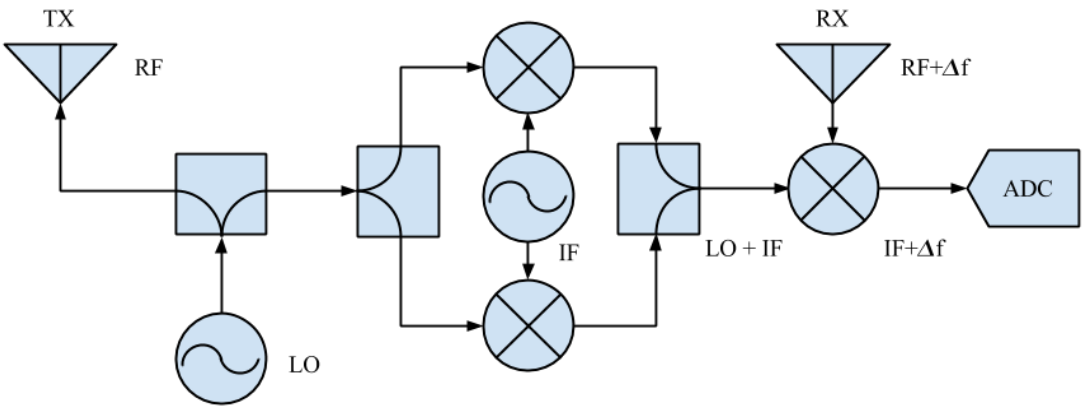

Fig. 8 Low-IF system block diagram

1.3.5 Inverse Digital Filter

Another method involves implementing an inverse digital filter in the processing of a dc-filtered signal [8]. This method is intended to restore the original signal rather than avoid the distortion caused by the filter. The transfer function of an inverse filter can be achieved simply by inverting the transfer function of a filter. Assuming the system consists of a first order digital high-pass filter with a transfer function expressed as

$$H(z) = \frac{b+1}{z} \times \frac{z-1}{z-b} \qquad \text{(Eq. 1.5)}$$

Simply by inverting the transfer function, the transfer function of the inverse filter can be expressed as

$$H_i(z) = \frac{1}{H(z)} = \frac{2}{b+1} \times \frac{z-b}{z-1} \qquad \text{(Eq. 1.6)}$$

Since this method is implemented in digital domain, there is no hardware modification required. However there are some disadvantages to use of this technique. First, since this method is implemented in the digital domain, it requires more computational resources. Second, the dc offset cannot be recovered by this process, because it is completely suppressed by the filter. Third, if there is a dc offset caused by the ADC, it is amplified by the inverse filter. Fourth, analog filters do not have the precise characteristics of a digital filter. Therefore, due to the variation of the each component, the design of an inverse filter may be challenging especially in the case of multiple channel systems.

1.4 Objectives of Study

As explained in the above sections, the dc offset caused by imperfection of the system hardware and external environment are problematic for the direct conversion system. At the same time, the dc offset caused by the detection subject is the vital information needed for accurate displacement detection. In this research, the dc offset optimization method based on theoretical and experimental analysis, and consideration of quadrature direct conversion system is studied. With this proposed method, the system can achieve dc information with decent amount of baseband gain, without causing saturation, without significant hardware modification, and without losing ADC dynamic range. Thus, it results in improving the capability and accuracy of human vital signs detection using a direct conversion system.

CHAPTER 2

FUNDAMENTAL THEORY

2.1 Doppler Effect

The Doppler effect is a phenomenon that causes frequency/pitch shift when the source of a signal and/or the observer move toward or away from each other. This phenomenon, as discovered by the German physicist Christian Doppler, applies to all wave motion including sound, light, and electromagnetic waves. The shifted frequency f' is called as Doppler shift and can be expressed as

$$f' = f\left(\frac{c + v_o}{c - v_s}\right) \qquad \text{(Eq. 2.1)}$$

where f is the frequency of source, c is the speed of light, v_o is the speed of receiver, and v_s is the speed of source.

To understand the Doppler effect, first assume that the frequency of a sound from a source is held constant. The wavelength of the sound will also remain constant. If both the source and the receiver of the sound remain stationary, the receiver will hear the same frequency sound produced by the source. This is because the receiver is receiving the same number of waves per second that the source is producing. If either the source or the receiver or both move toward the other, the receiver receives higher frequency sound due to receiving a greater number of sound waves per second. Thus, it results in increasing the frequency of sound. Alternatively, if the source and the receiver are moving apart, the receiver receives a smaller number of sound waves per second that results in decreasing

the frequency of sound. In both cases, the frequency of the sound produced by the source will have remained constant.

2.2 Doppler Radar Principle

Doppler radar can detect the position and velocity of the target by measuring the Doppler shift described in the previous section. When the target is going away from the radar, the frequency of the reflected signal by the target is decreased by Doppler effect. On the other hand, when the target is coming closer to the radar, the frequency of reflected signal is increased. By measuring this frequency shift, the radar system can detect the speed of the subject moving toward the radar. In the case of detecting the displacement information, the motion causes phase shift instead of frequency shift. In Fig. 9, the basic theory of the Doppler radar transceiver system for displacement detection is shown. In transceiver configuration, the transmitting and receiving path are isolated by a duplexing component, such as a magnetic circulator. Assuming there is no phase noise in the system, the local oscillator signal LO is represented by

$$T(t) = \cos(2\pi f_t t) \qquad \text{(Eq. 2.2)}$$

where f_t is the frequency of the transmitting signal. When a radar system transmits the signal, a small portion of that energy is reflected by the subject. The signal is received by the antenna, and can be represented by

$$R(t) = \cos(2\pi f_t t + \theta + p(t)) \qquad \text{(Eq. 2.3)}$$

where q is the constant phase shift, and $p(t)$ is the time varying phase shift caused by the movement of the target. After mixed the LO signal and received signal, the movement information of target can be expressed as [9]

$$B(t) = \cos(q + p(t) + \mathrm{D}f(t)) \qquad \text{(Eq. 2.4)}$$

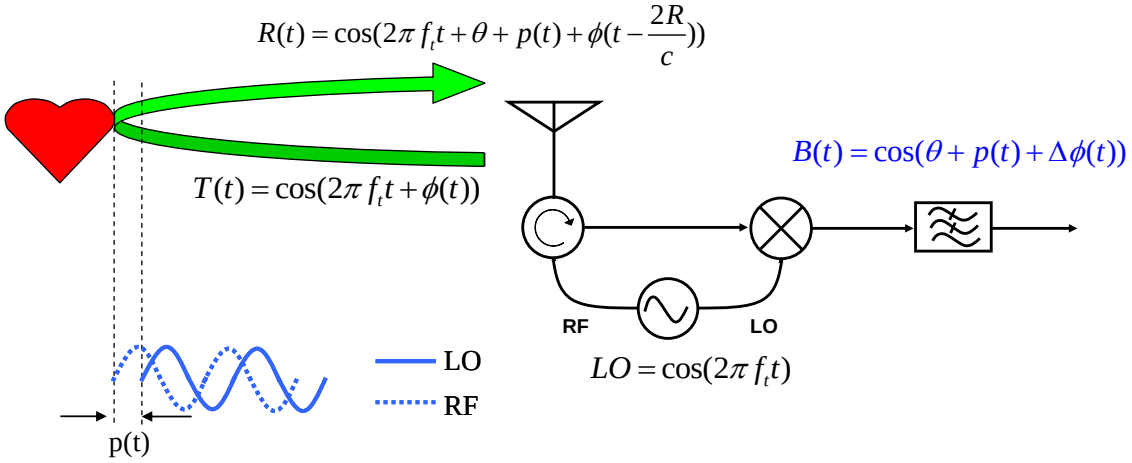

Fig. 9 Basic Principle of Doppler Radar

2.3 Radar Equation

The range on radar techniques is defined as the distance from the radar system to the subject measured along the line of sight. If the respective running time t is known, then the distance R can be calculated by using "Radar range equation" which is used to estimate the received power in a radar system. The estimation is based on the physical dependences of the transmit power, that is the wave propagation up to the receiving of the echo-signals.

If an electromagnetic energy is transmitted by an isotropic antenna, then the energy is propagated uniformly in all directions. Thus, the energy density spreads

spherically and at the point of distance R from the radar, and the total power will be distributed across the surface A:

$$A = 4\pi R^2 \qquad \text{(Eq. 2.5)}$$

The same amount of energy is radiated on an incremented spherical surface; thus the power density on the surface of a sphere is inversely proportional to the radius of the sphere. This Power Density S_i can be expressed as

$$S_i = \frac{P_t}{4\pi R_1^2} \qquad \text{(Eq. 2.6)}$$

where P_t is transmitted power in watt, and R_1 is the distance between antenna to subject in meters. If the transmitting antenna has directivity instead of uniform radiation, the directional power density can be expressed as

$$S_g = S_i \cdot G \qquad \text{(Eq. 2.7)}$$

where S_g is the directional power density, and G is the antenna gain. The target detection does not only depend on the power density at the target position, but also on how much power is reflected from the target. In order to estimate the reflected power, it is necessary to know the radar cross section described in the previous section. This quantity depends on various factors, but in general a bigger area reflects more power than a smaller area. The reflected power P_d at the radar depends on the power density S_i, the antenna gain G, and the radar cross section σ:

$$P_d = S_g \sigma = \frac{P_t G \sigma}{4\pi R_1^2} \qquad \text{(Eq. 2.8)}$$

Since the reflected signal can be presumed as the same condition as the transmitted signal, the power density yielded at the receiver S_r is given by:

$$S_r = \frac{P_d}{4\pi R_2^2} \quad \text{(Eq. 2.9)}$$

where R_2 is the distance between the target to receiving antenna in meter. Taking into account the internal signal losses in antenna, the received power can be expressed as

$$P_r = S_r A\eta = S_r A_e \quad \text{(Eq. 2.10)}$$

where A_e is the effective antenna area, A is the physical antenna area, and η is the antenna efficiency. From equation 2.8, 2.9 and 2.10, the received power is then calculated as

$$P_r = \frac{P_d A_e}{4\pi R_2^2} = \frac{P_t G\sigma A_e}{(4\pi)^2 R_1^2 R_2^2} \quad \text{(Eq. 2.11)}$$

Presuming the radar system is composed as a transceiver, the range R_1 (from antenna to target) is equal to R_2 (from target to Antenna). Then the equation 2.11 is expressed as

$$P_r = \frac{P_t G\sigma A_e}{(4\pi)^2 R^4} \quad \text{(Eq. 2.12)}$$

Since the antenna gain is proportional to the antenna aperture, the effective antenna area can be expressed with antenna gain G and wavelength λ

$$A_e = \frac{G\lambda^2}{4\pi} \quad \text{(Eq. 2.13)}$$

Replacing this into equation 2.12, it yields

$$P_r = \frac{P_t G^2 s \lambda^2}{(4\pi)^3 R^4} \quad \text{(Eq. 2.14)}$$

Solving for range R, the radar range equation can be expressed as

$$R = \sqrt[4]{\frac{P_t G^2 \lambda^2 s}{P_r (4\pi)^3}} \quad \text{(Eq. 2.15)}$$

All quantities that influence the wave propagation of radar signals were taken into account in this equation. By assuming the smallest received signal that can be detected as P_{rmin}, the maximum detectable range can be estimated as

$$R_{\max} = \sqrt[4]{\frac{P_t G^2 \lambda^2 s}{P_{r\min} (4\pi)^3}} \quad \text{(Eq. 2.16)}$$

2.4 Radar Cross Section

A Doppler radar system can obtain the information of the moving subject by receiving and analyzing the reflected signal by the subject. In general, such reflected wave is known as back-scatter. In radar techniques, the intensity of back-scatter is quantified and represented as the radar cross section σ. The definition of the radar cross section can be expressed as

$$s = 4\pi R^2 \frac{|E_r|^2}{|E_i|^2} \quad \text{(Eq. 2.17)}$$

where R is the range, E_r is the electric field strength of reflected signal, and E_i is the electric field strength of incident signal. In Fig. 10, the radar cross section of a sphere is shown.

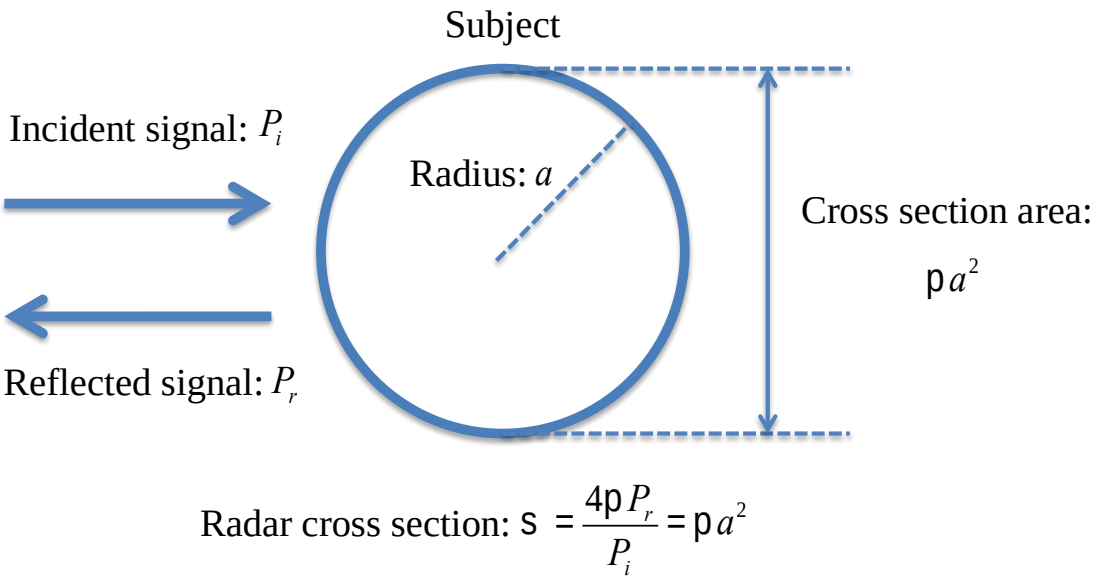

Fig. 10 Radar Cross Section

2.5 Quadrature System

In Fig. 9, a single channel Doppler radar architecture is shown and the output signal obtained by the system is expressed by equation 2.4. This output signal only represents the time varying phase shift. Applying the complex analysis, the phase information can be represented by the argument on a complex plane. In Fig. 11, an image of the time varying phase shift and the phase information on a complex plane is shown.

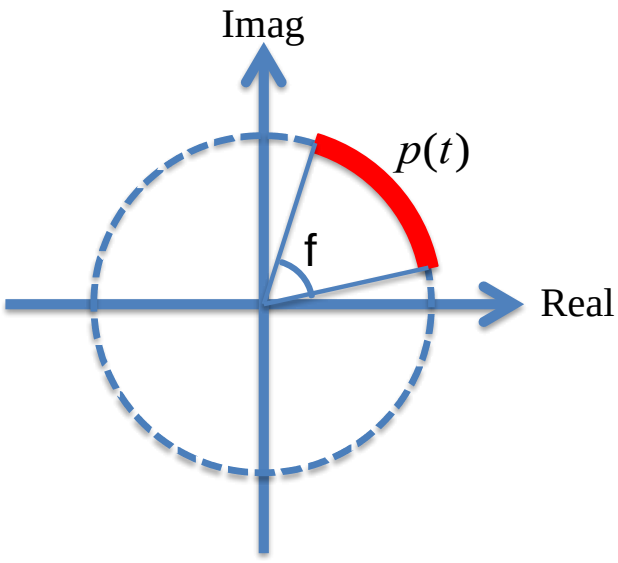

Fig. 11 The time varying phase shift and the phase on complex plot

Based on this image, the phase information ϕ can be represented by the argument of two signals, which have a 90-degree phase difference (i.e. Real and Imaginary). In order to realize this in a Doppler radar system, an extra channel is introduced, and the system block diagram is shown in Fig. 12. A 90-degree power splitter is introduced in the receiver chain that splits the received signal to create the phase difference. Since the two output signals contain a 90-degree phase difference, the original channel is known as the in-phase (I) channel, another channel is known as the quadrature (Q) channel, and hence this architecture is called a quadrature direct conversion system. Due to the phase difference, those two signals can be represented by sine and cosine functions and can be expressed by Euler's formula

$$B_I(t) + jB_Q(t) = \cos(q + p(t)) + j\sin(q + p(t)) = e^{j(q+p(t))} \qquad \text{(Eq. 2.18)}$$

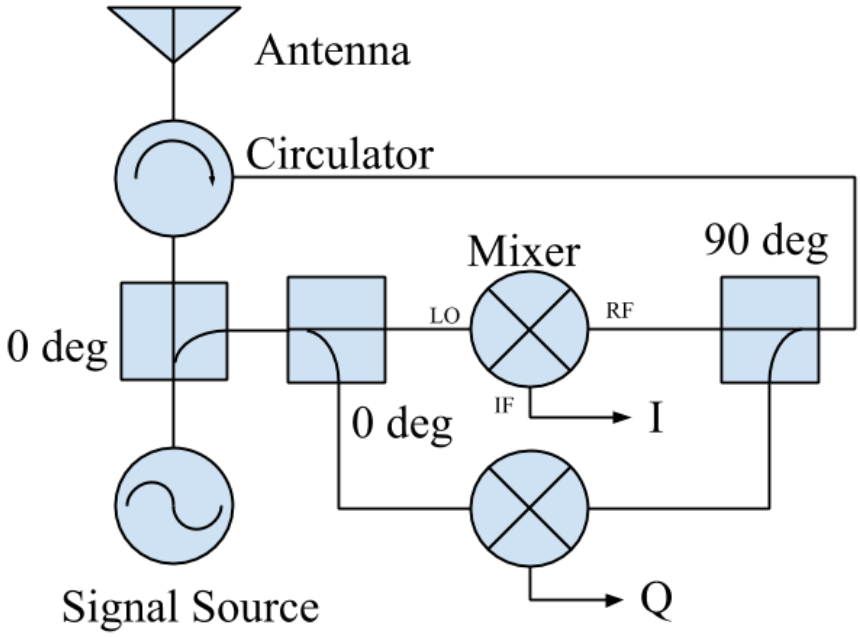

Fig. 12 Block diagram of quadrature Doppler radar transceiver

2.6 Phase Demodulation Process

The baseband output signal in a single channel configuration is essentially proportional to the phase change, and can be directly used for estimating human vital signs. No further phase demodulation is required, nor possible in this case. In order to achieve the phase information, a quadrature system is commonly used, as described in the previous section. The phase information can be obtained from the quadrature outputs with a proper method to combine *I* and *Q* channels. This process is called demodulation. There are several methods available to demodulate the *I* and *Q* channels and described two major methods in this section.

2.6.1 Linear Demodulation

The first method is known as linear demodulation. With this demodulation process, basically the two dimensional data is projected into a single dimension. This demodulation method utilizes the property of eigenvector and covariance matrix; therefore it is also called as eigenvector demodulation. Steps for this linear demodulation are:

1) Remove the mean value of both I and Q signals
2) Calculate the covariance matrix of the I and Q signals.
3) Calculate eigenvectors and eigenvalues of the covariance matrix,
4) Multiply the eigenvectors with the data, and pick the output with largest variance

Graphically, this can be explained by rotating the arc of IQ data such that it will be in line with one of the axes resulting in maximum amplitude of signal, which can be taken as the demodulated signal (Fig. 13).

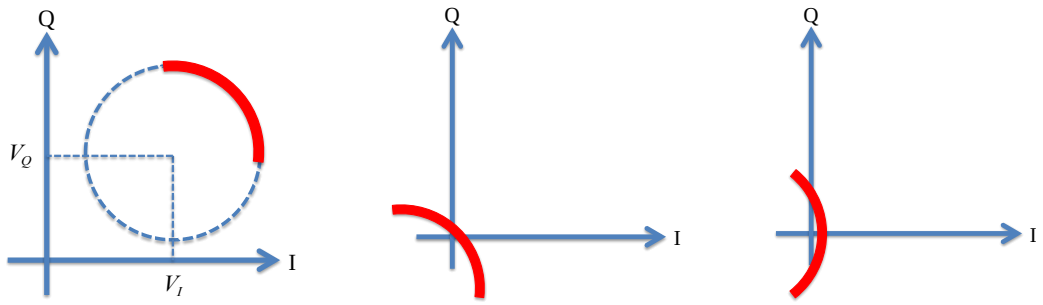

(a) Raw data (b) DC removed data (c) Rotated (demodulated) data

Fig. 13 Plots illustrating the principle for linear demodulation

2.6.2 Non-linear Demodulation

The main assumption for using linear demodulation is that the arc of *IQ* signals is very small such that it can be approximated with a straight line. This assumption may not always be valid if the motion has a larger displacement or the carrier signal is a higher frequency, in which situations result in a longer arc length in the *IQ* plane. In such cases, linear demodulation cannot yield optimum results, and a nonlinear method must be used. In addition, only nonlinear demodulation can provide absolute displacement. Thus, it is required for accurate displacement detection. Since the quadrature outputs have a 90-degree phase difference, and each signal can be expressed as sine and cosine functions, the phase information can be obtained by taking the ratio between two outputs and applying the arctangent function. This demodulation process can be expressed as

$$f(t) = \arctan\left(\frac{B_Q}{B_I}\right) = \arctan\left(\frac{A_r \sin(q + p(t))}{A_r \cos(q + p(t))}\right) = q + p(t) \qquad \text{(Eq. 2.19)}$$

Since this method utilizes the property of arctangent function, it is also known as arctangent demodulation [4].

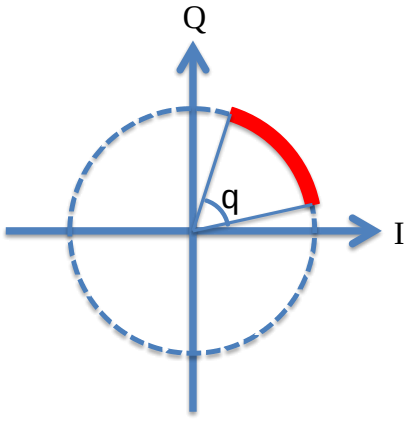

Fig. 14 Arctangent demodulation process

CHAPTER 3
RESEARCH APPROACH

3.1 Assessment of dc offset

In a direct conversion system, there is dc offset caused by imperfection of the system (Internal dc offset), the environment around the system (clutter dc offset), and the detection subject (dc information). In order to obtain an accurate demodulation signal, these dc offsets have to be carefully managed. First, in order to identify the magnitude of these dc offsets, several measurements are executed. In Fig. 15, measured averaged dc offset of IQ direct conversion system is shown. In this measurement, the averaged dc offset level of an RF signal absorber, without the absorber, human subject, and linear actuator placed in front of radar system were measured.

When an RF absorber is placed in front of radar system, a “With absorber” case, 23.2mV (I channel) and -97mV (Q channel) of dc offset is achieved. Since the absorber avoids any signal reflection, there is no external dc offset in this case. In other words, all of this dc offset is the internal dc offset caused by the imperfection of this radar system.

In a case of “Without absorber”, 22.6mV (I channel) and -98.57mV (Q channel) was achieved. In this case, the dc offset level of both channels are slightly differed from the “with absorber” case, since the external environment reflects portion of signal and introduces external dc offset in the system.

In a case of “With subject”, 23.64mV (I channel) and -95.83mV (Q channel) was achieved. In this case, in addition to the clutter dc offset, the dc information created by the subject that is vital information for non-linear demodulation is introduced.

In a case of “With Linear actuator”, 23.18mV (I channel) and -98.46mV (Q channel) was achieved. This case is same as “With subject” case. Thus the dc offset contains the internal and external dc offset as well as dc information.

In Table 1, the differences between each of the cases are shown with “With absorber” case as reference dc offset level. From this comparison, since the case “With absorber” only contains internal dc offset, the dc offset induced by external environment and detection subjects are very small. Thus, the majority of the dc offset in the system is the internal dc offset caused by the system imperfection.

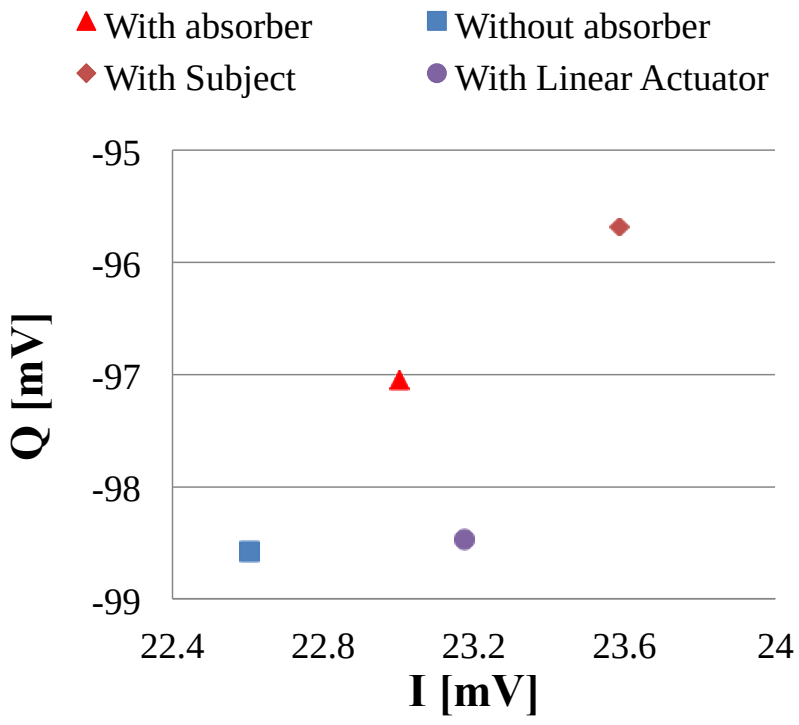

Fig. 15 Averaged dc offset levels

Table 1 DC offset level differences ("With absorber" case as the reference)

	I [mV]	Q [mV]
Without absorber	-0.40	-1.53
With subject	0.59	1.36
With linear actuator	0.17	-1.42

In Fig. 16, the one way free space path loss at 2.4GHz is shown. If a target or clutter is placed a few meters from the radar system, it only generates small amount of the self-mixing signal due to the free space losses. These measurement results and analysis indicate that the internal dc offset is significantly larger than external dc offset. If the internal dc offset is reduced or compensated, the system can achieve dc coupled signal with decent amount of baseband gain without making saturation and without losing ADC dynamic range.

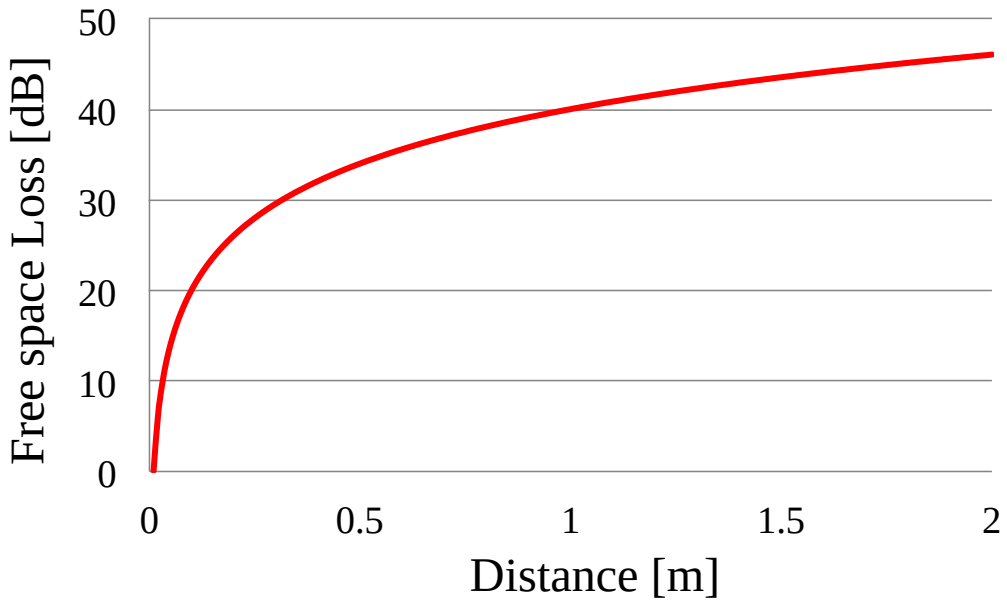

Fig. 16 One-way free space path loss at 2.4GHz

3.2 Analysis of Internal DC Offset

In order to understand the issues, in this section, the internal dc offset caused by the imperfection of the direct conversion system hardware, and the external environment is thoroughly analyzed and described.

3.2.1 Mixer DC Offset

Fig. 17 shows the measured dc offset of a mixer. In this measurement, the RF port was connected to 50Ω and measured dc offset output from IF port while +7dBm of LO signal is injected to LO port. From this result, the mixer induces 20mV of the dc offset even with the RF port terminated with 50 Ω. Thus, just driving a mixer with LO signal induces dc offset to its output because of self-mixing happening internally.

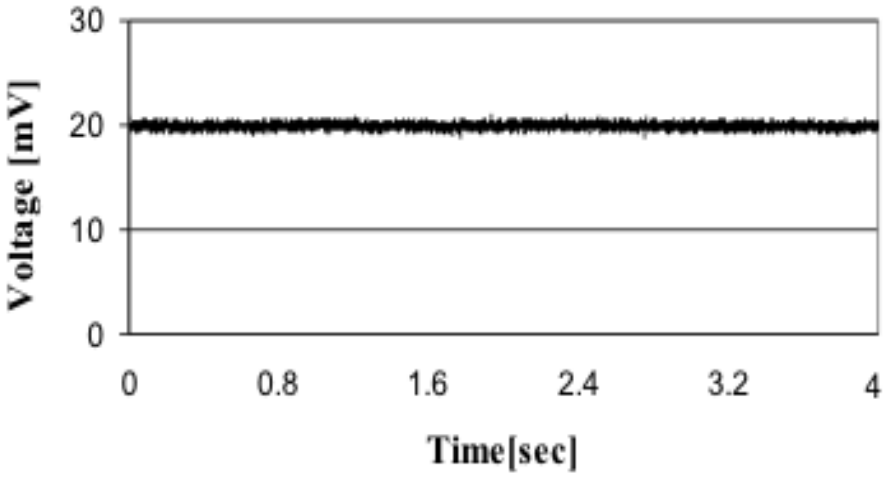

Fig. 17 Measured dc offset at mixer IF port

3.2.2 LO Leakage DC Offset

There is an issue of leakage from the Tx to the Rx in transceiver configuration due to finite isolation of the circulator. Because the Tx leakage signal is delivered to the mixer RF port, it results in a self-mixing signal, which induces dc offset. The amplitude of this dc offset depends on the magnitude of the leakage and phase relationship between LO and leakage; thus it depends on the Tx-Rx isolation, path loss, and electrical length of LO and RF paths. In order to see the effect of the phase relationship, a phase shifter (Pulsar ST-21-444A) was installed in the Rx path to adjust the phase of the leakage, and the dc offset was measured with an oscilloscope connected to the IF port of the mixer. In Fig. 18, the measured dc offset result is shown. The maximum and minimum dc offset levels observed were 67mV and 6mV, respectively. This result shows that the optimum case and worst case in direct conversion transceiver exist since the dc offset level depends on the phase relationship between LO and the leakage signals.

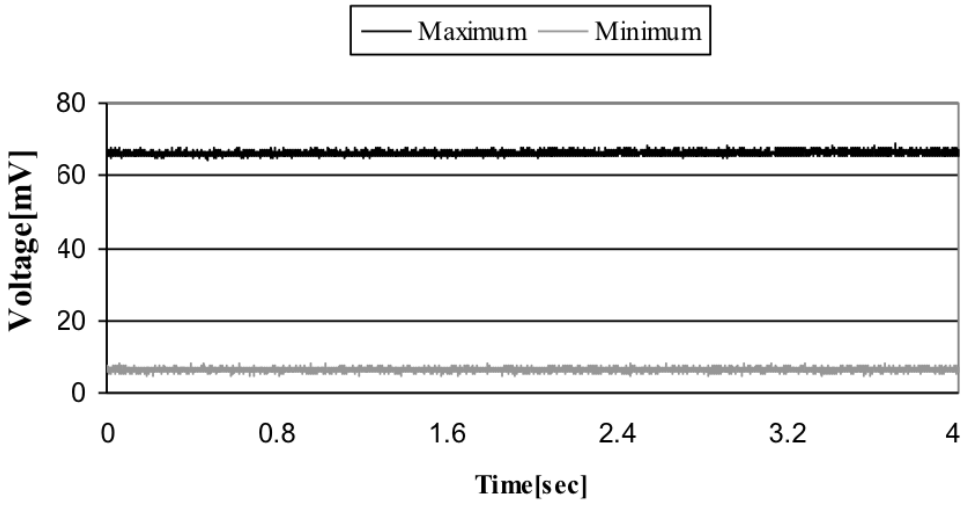

Fig. 18 Measured dc offset of direct conversion transceiver

In Fig. 19, measured dc offset of the quadrature transceiver is shown. In addition to the single channel system, the quadrature system produces I and Q signals, which have a 90-degree phase difference with each other. Thus the LO leakage from two mixers also has a 90-degree phase difference, meaning the phase relationship between LO and leakage signal of I and Q channels also has a 90-degree phase difference.

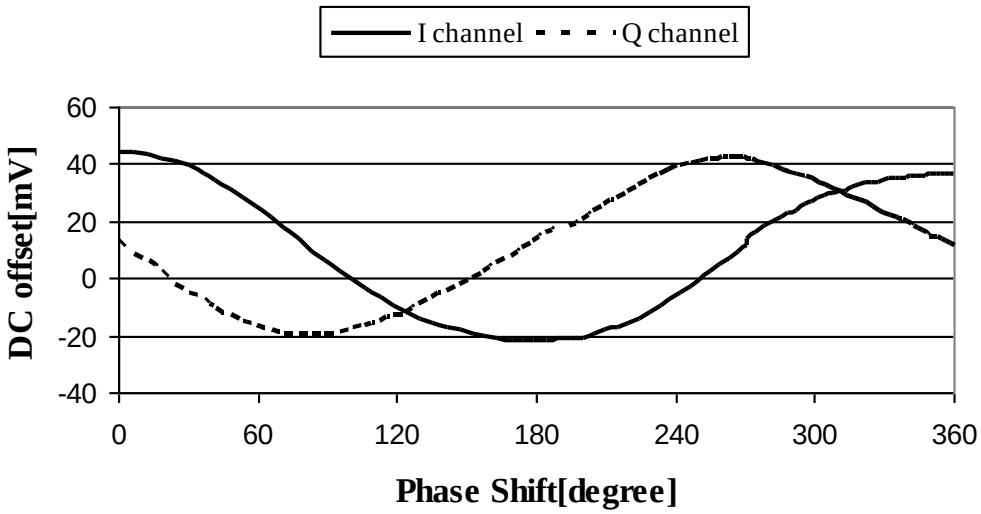

Fig. 19 DC offset of I and Q channel

3.2.3 Total DC Offset

Assuming the target's motion variation is given by $\Delta x(t)$, the quadrature baseband output assuming balanced channels can be expressed as:

$$s(t) = V_r + A_r \exp\left[q + 4\pi\Delta x(t)\right] \qquad \text{(Eq. 3.1)}$$

where V_r is the internal and external dc offset and θ is the constant phase shift related to the phase change at the surface of a target and the phase delay between the mixer and antenna. From this equation, the total dc offset of the system V_{dc} is expressed as:

$$V_{dc} = V_r + A_r \exp(q) \qquad \text{(Eq. 3.2)}$$

Based on the analysis in the previous section, the internal and external dc offset V_r contains mixer dc offset, self-mixing (Internal) dc offset, and clutter (external) dc offset; therefore it can be expressed as:

$$V_{dc} = V_{mixer} + B_r \exp(\phi_{leak}) + C_r \exp(\phi_{ext}) + A_r \exp(\theta) \qquad \text{(Eq. 3.3)}$$

Where ϕ_{leak} is the phase of leakage and ϕ_{ext} is the phase due to the distance between clutter and radar system. If the hardware is not reconfigurable, the internal dc offset terms V_{mixer} and $B_r \exp(\phi_{leak})$ are constant. On the other hand, the external dc offset $C_r \exp(\phi_{ext})$ and dc information $A_r \exp(\theta)$ are varied by the environment, radar cross-section and the placement of the subject. Based on this analysis, an image of dc offset on quadrature direct conversion system is shown in Fig. 20.

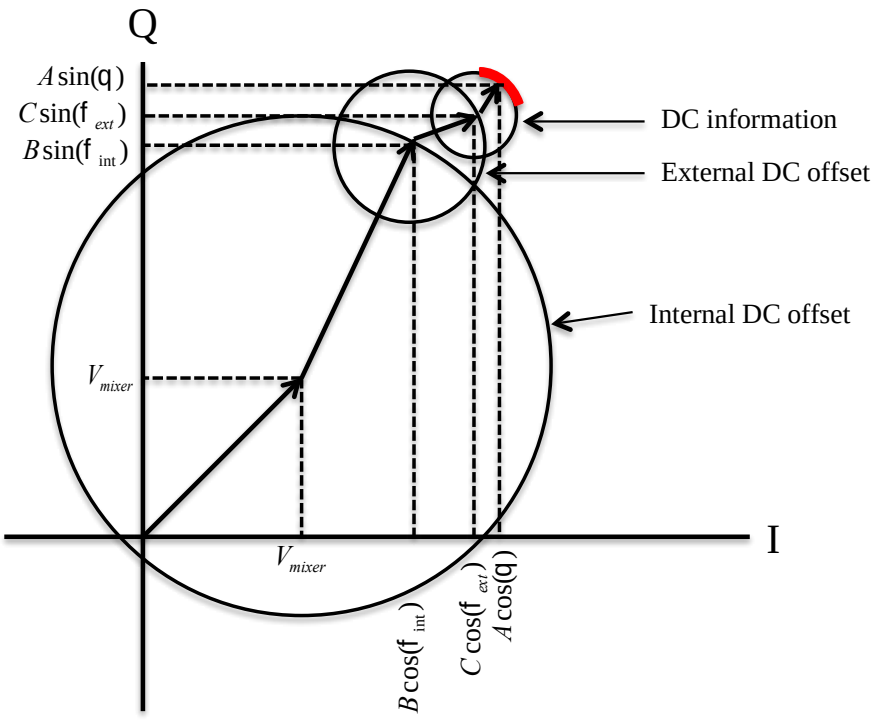

Fig. 20 The dc offset of quadrature direct conversion system

CHAPTER 4
DC OFFSET OPTIMIZATION

Based on measurement and analysis, in this chapter, two proposed dc offset optimization methods are described. Since the majority of dc offset is caused by system imperfections, which is a constant, the dc coupled system with a decent amount of baseband gain without causing saturation can be realized by cancelling the internal dc offset.

4.1 DC Offset Optimization

In Fig. 21, a block diagram of proposed dc coupled quadrature direct conversion system is shown. In addition to the existing system, a phase shifter is installed in between two 0-degree power splitters in Tx path, and a dc power source to supply a cancelling dc to differential input port of the baseband amplifier. In the calibration process, to avoid any external dc offset, a RF absorber is placed in front of the antenna. The phase of the LO leakage signal is adjusted to create the same amount of dc offset for both I and Q channels by making the ϕ_{leak} to either 45° or 225°. Only at these two angles, one dc power source can cancel the dc offset of both channels. Also, it avoids flicker noise imbalance caused by having different dc offset levels in each channels. After the dc offset is adjusted, it is cancelled by applying the same amount of dc to the differential input of the baseband amplifier. Since these processes remove all the internal dc offset, it is possible to increase the baseband gain without causing saturation. Thus, this system can

realize the dc coupled direct conversion system with a decent amount of baseband amplifier gain.

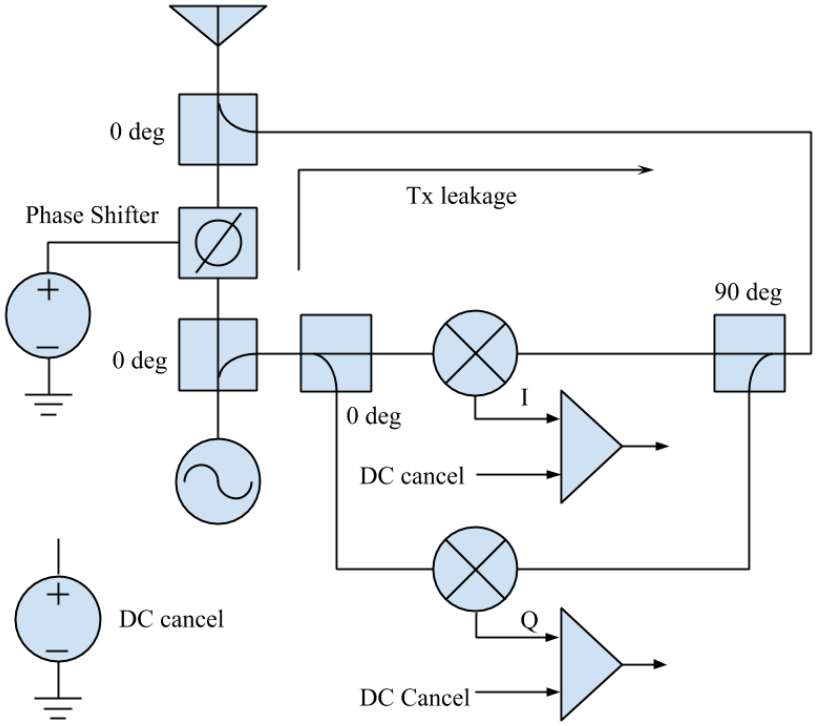

Fig. 21 The block diagram of dc coupled quadrature direct conversion system

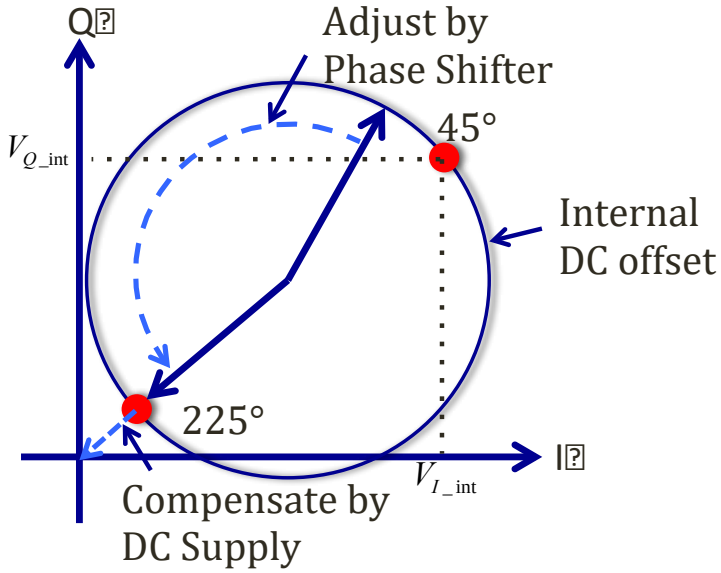

Fig. 22 DC offset compensation process

Using this proposed technique, breathing of a human subject is measured. The distance between the subject and the antenna is about 1 meter. In Fig. 23, the measured result is shown.

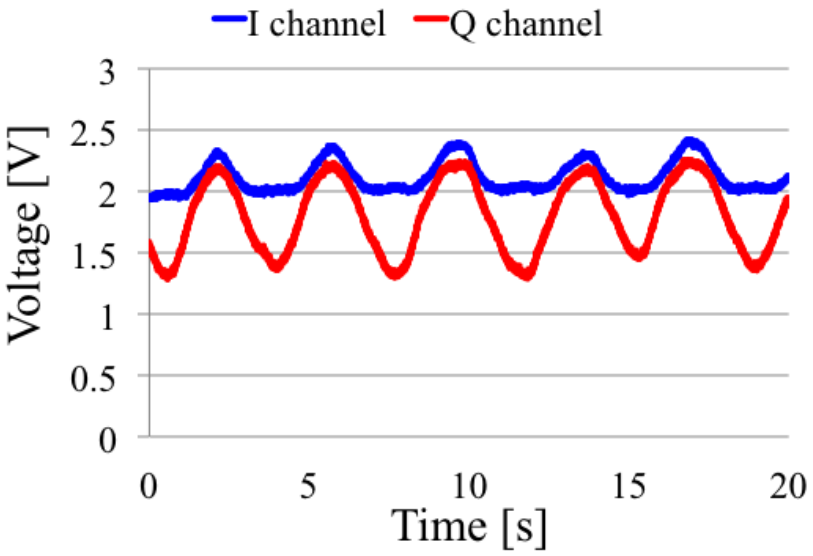

(a) Raw data

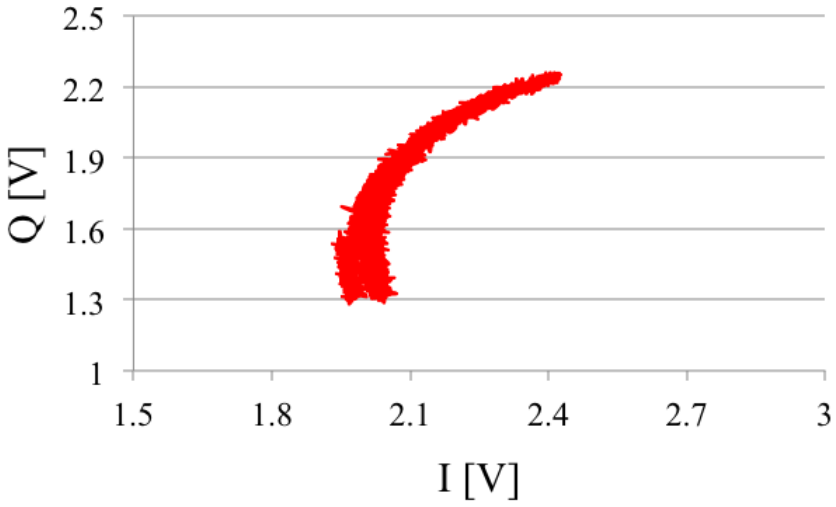

(b) IQ plot

Fig. 23 The measured results of human breathing

In order to demonstrate the effectiveness of this dc offset optimization technique, several different types of motions created by a linear actuator are measured and compared with the proposed system and conventional ac coupling system. The measurement system setup is shown in Fig. 24. In this system, the output signal from I and Q channels are split into two, and one is configured as the proposed dc coupled system using the method explained, and another is configured as the ac coupled system which consists of 0.03-30 Hz band-pass filter. The gain of the baseband amplifier is 1000 for both AC and DC coupled methods.

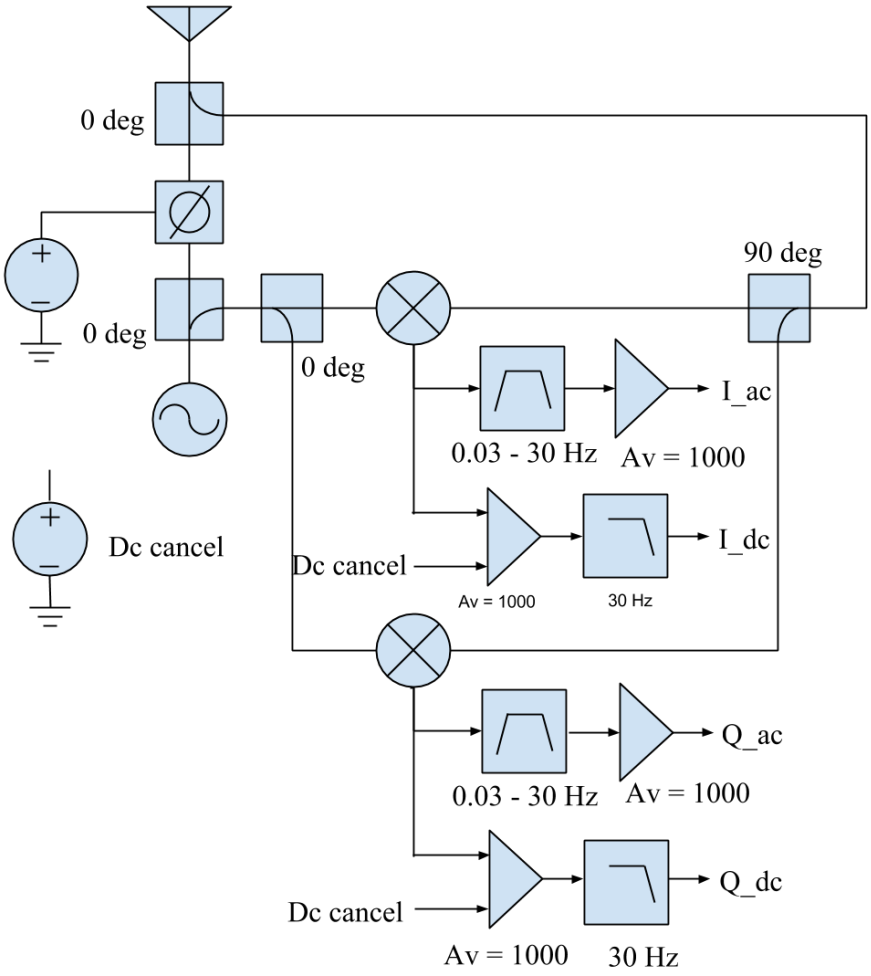

Fig. 24 Block diagram of AC/DC coupled system

In Fig. 25, the measurement result without any motion is shown (Empty room). Due to the filter, there is no dc offset in the ac coupled result (a). On the other hand, there is about 3V and 1.5V of dc offset in the dc coupled system. This is due to the small dc offset caused by the external environment. Although it creates a large amount of dc offset due to the amplifier, it still does not cause the saturation.

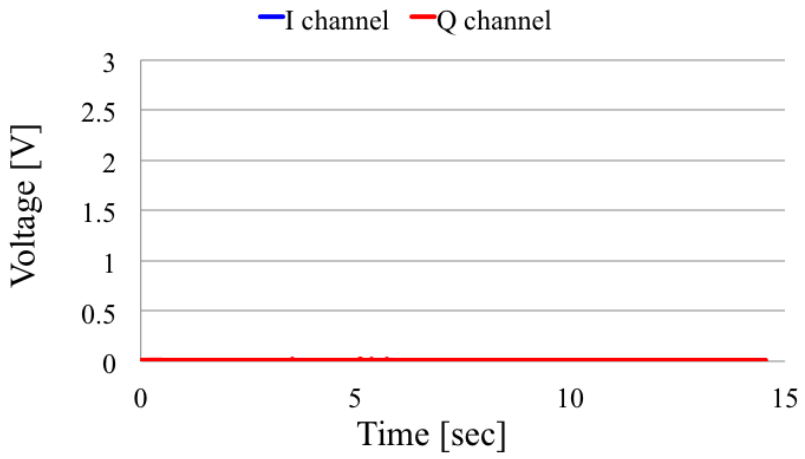

(a) AC coupled

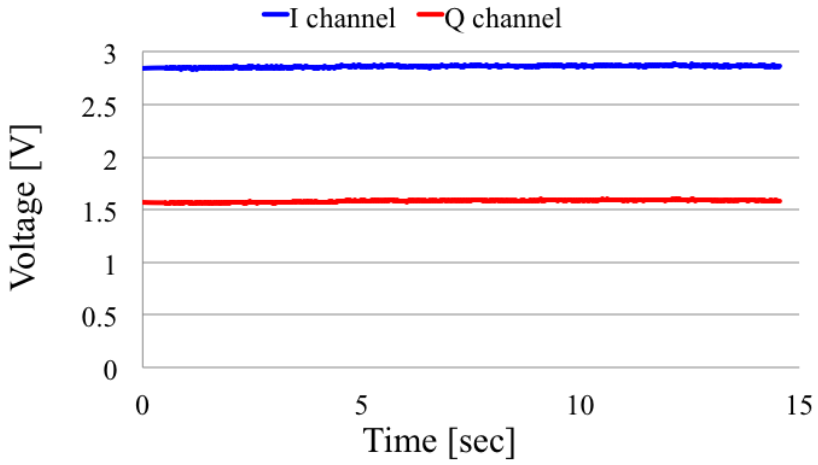

(b) DC coupled

Fig. 25 Measured results (Empty room)

In Fig. 26, the measured results when the target moves with 1cm of displacement with 0.4Hz are shown. Fig. 27 and Fig. 28 show the IQ plot and arctangent demodulated signals respectively. These results show that the dc coupled system can achieve almost the same result as the ac coupled system without causing saturation.

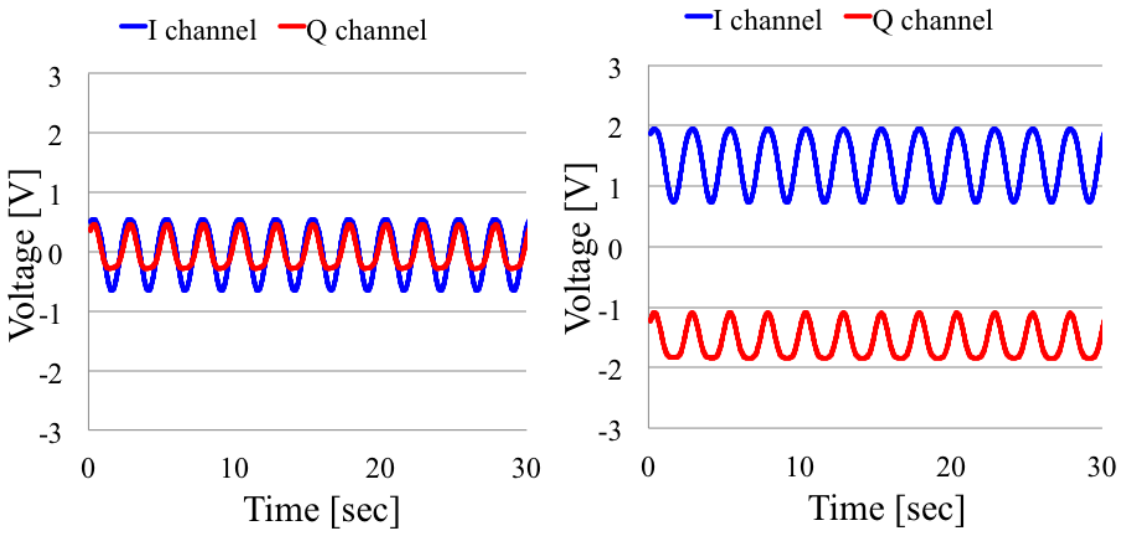

(a) AC coupled (b) DC coupled

Fig. 26 Measured results (0.4Hz 1cm displacement)

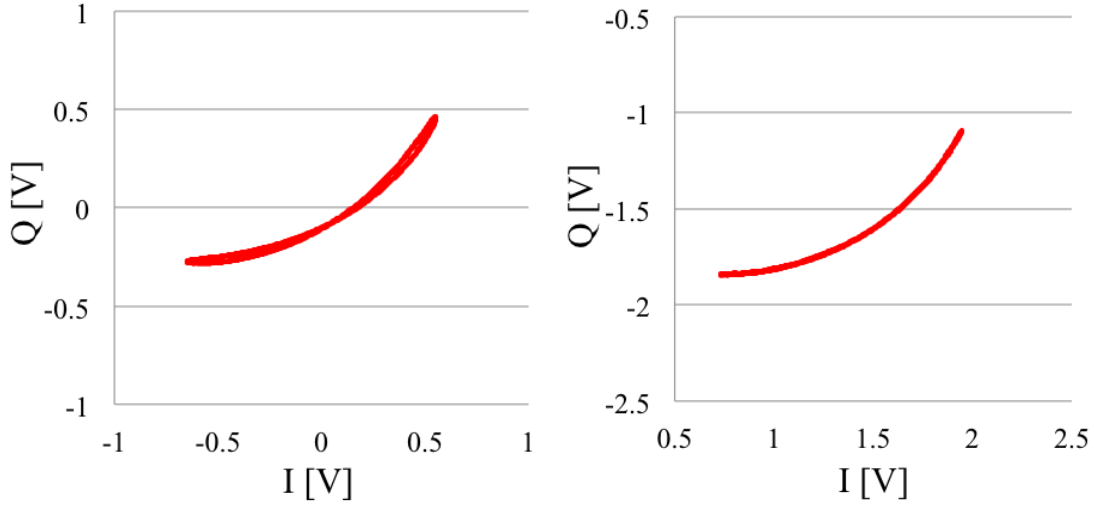

(a) AC coupled (b) DC coupled

Fig. 27 IQ plot (0.4Hz 1cm displacement)

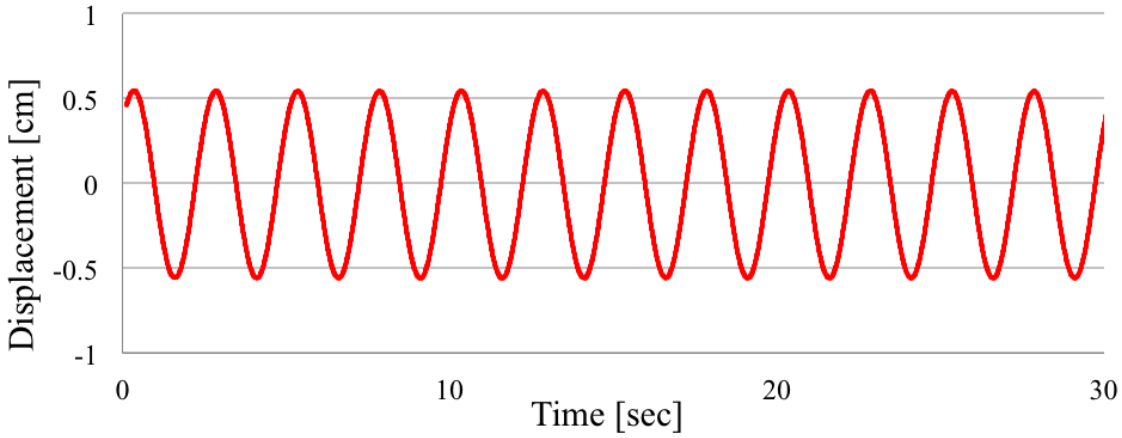

(a) AC coupled

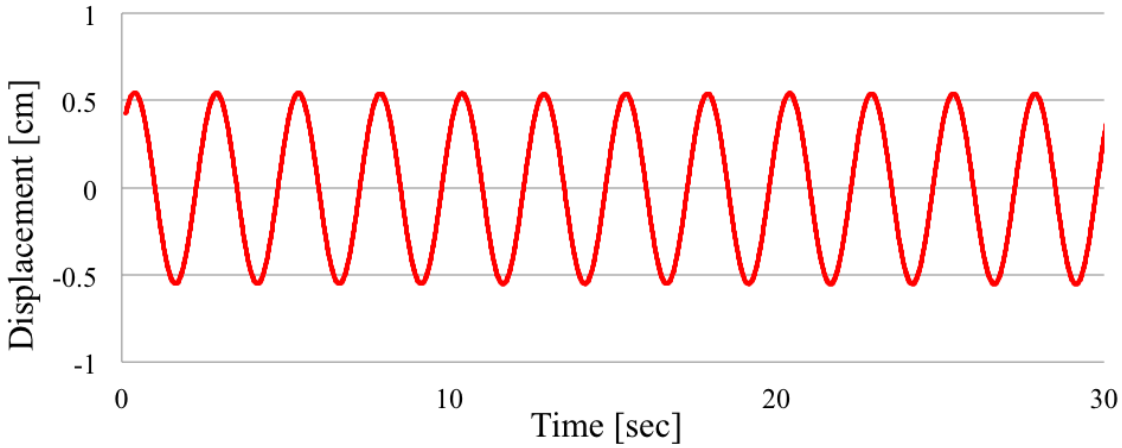

(a) DC coupled

Fig. 28 Arctangent demodulated signal

In Fig. 29, the measured results when the target moves with 1cm of displacement with 0.04Hz are shown. Fig. 30 and Fig. 31 show the IQ plot and arctangent demodulated signals respectively. These results show that the ac coupled system distorts the signal since the frequency of the signal is outside of the pass band. On the other hand, the dc coupled system achieves the demodulated signal accurately without causing any distortion.

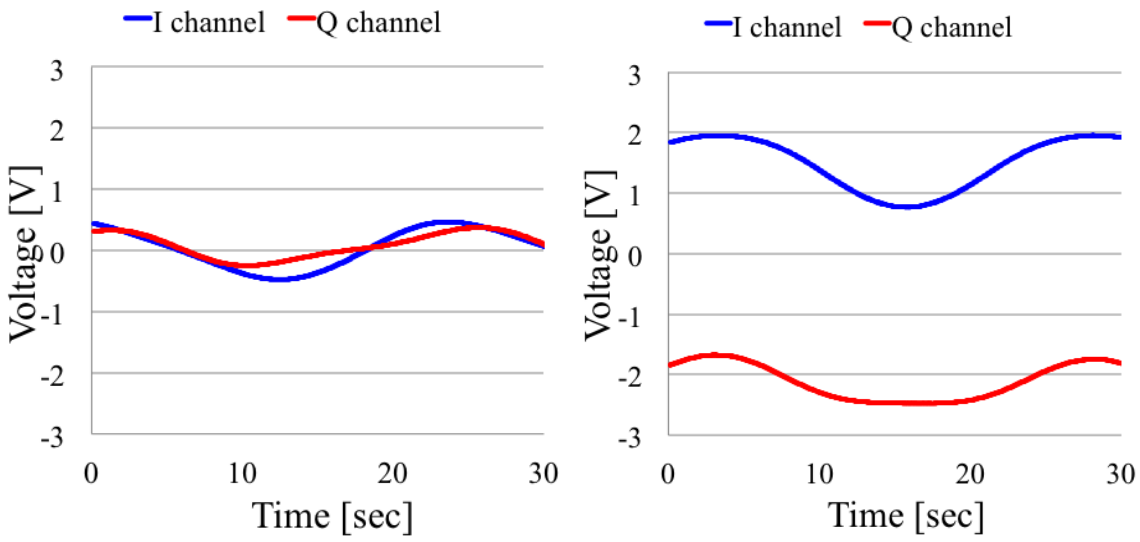

(a) AC coupled (b) DC coupled

Fig. 29 Measured results (0.04Hz 1cm displacement)

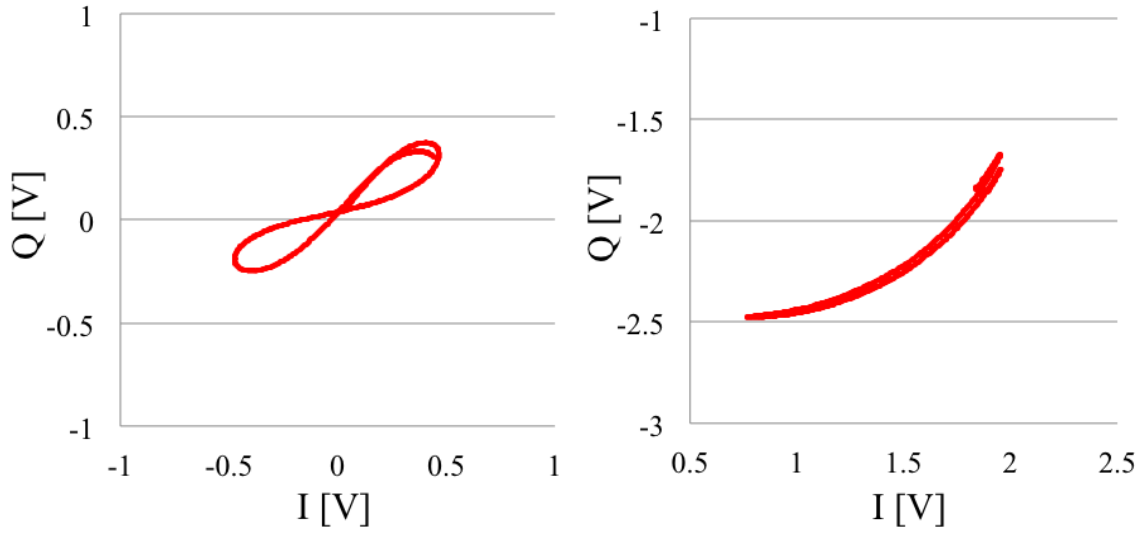

(a) AC coupled (b) DC coupled

Fig. 30 IQ plot (0.04Hz 1cm displacement)

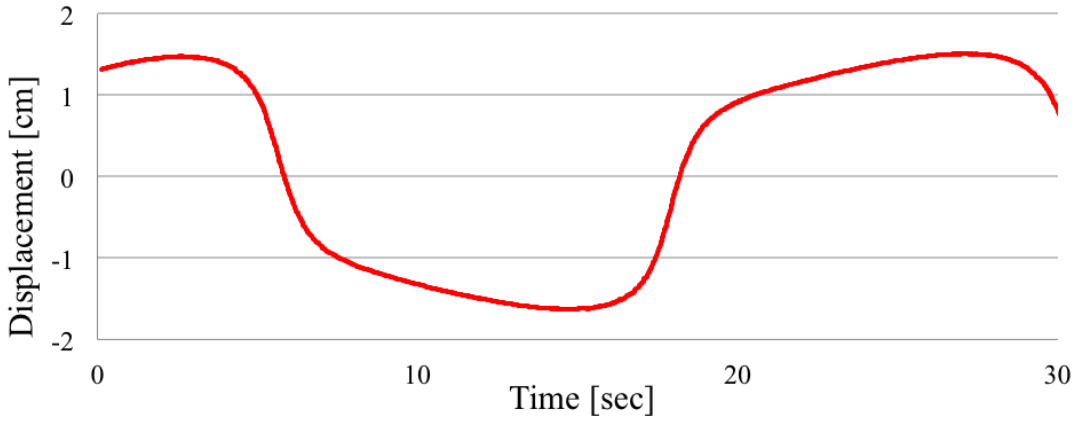

(a) AC coupled

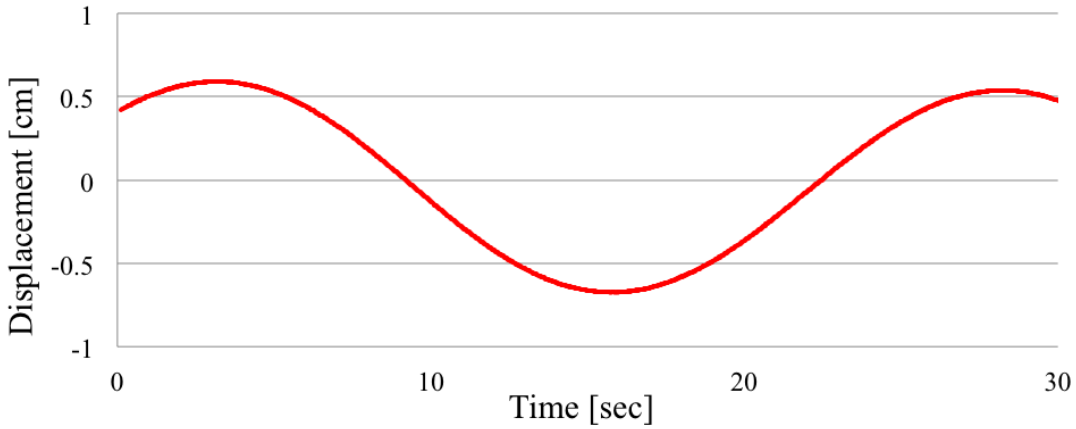

(b) DC coupled

Fig. 31 Arctangent demodulated signal

In Fig. 32, the measured results when the target moves with 1cm of displacement with 0.01Hz are shown. Fig. 33 and Fig. 34 show the IQ plot and arctangent demodulated signals respectively. These results show that the ac coupled system distorts the signal since the frequency of the signal is outside the pass band. On the other hand, the dc coupled system achieved the demodulated signal without any distortion.

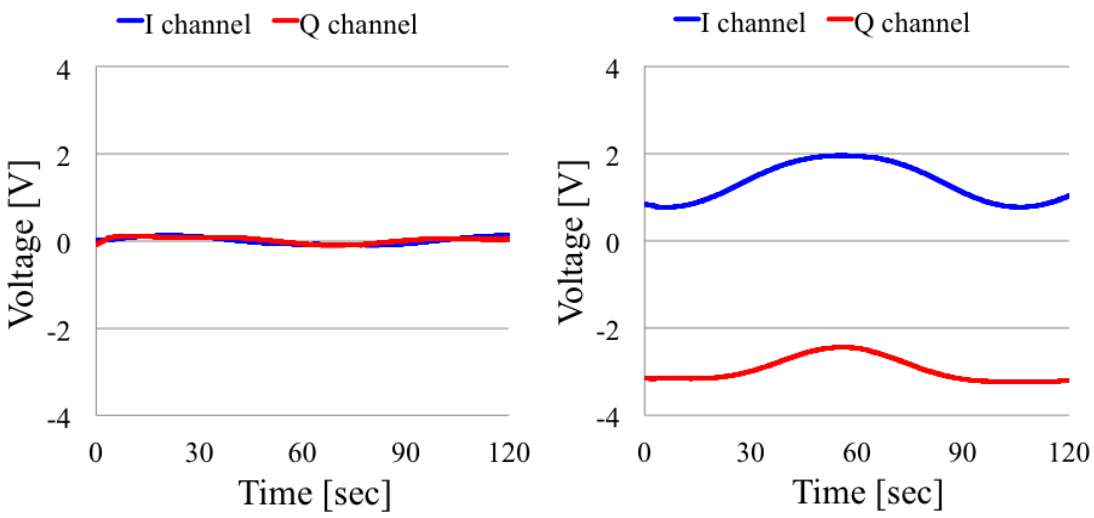

(a) AC coupled (b) DC coupled

Fig. 32 Measured results (0.01Hz 1cm displacement)

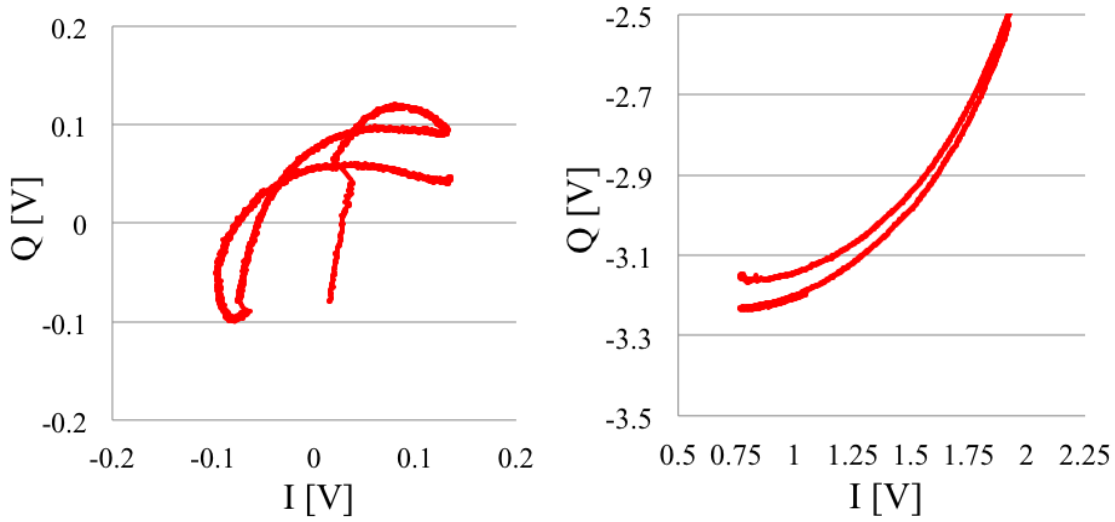

(a) AC coupled (b) DC coupled

Fig. 33 IQ plot (0.01Hz 1cm displacement)

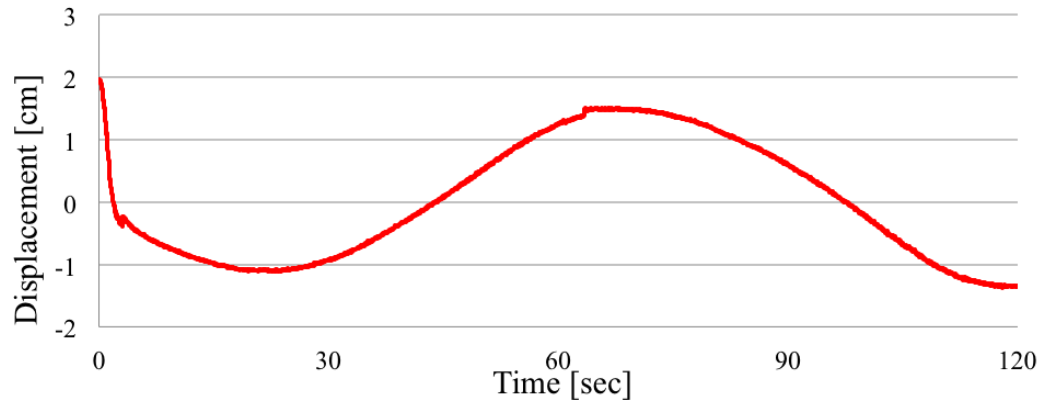

(a) AC coupled

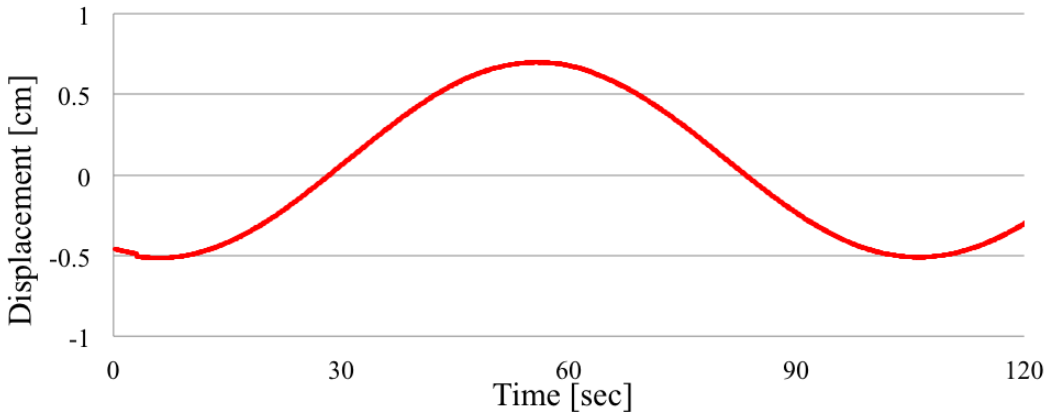

(b) DC coupled

Fig. 34 Arctangent demodulated signal

In order to demonstrate the effectiveness of the dc coupled system and the effect of the filter, a step motion is measured. The sequence of the motion is; 1cm move forward followed by 10 seconds stay, then another 1 cm move forward followed by 10 seconds stay, then 1 cm move backward followed by 10 seconds stay, and then 1cm move backward. In Fig. 35, the motion of linear actuator of step motion measurement is shown.

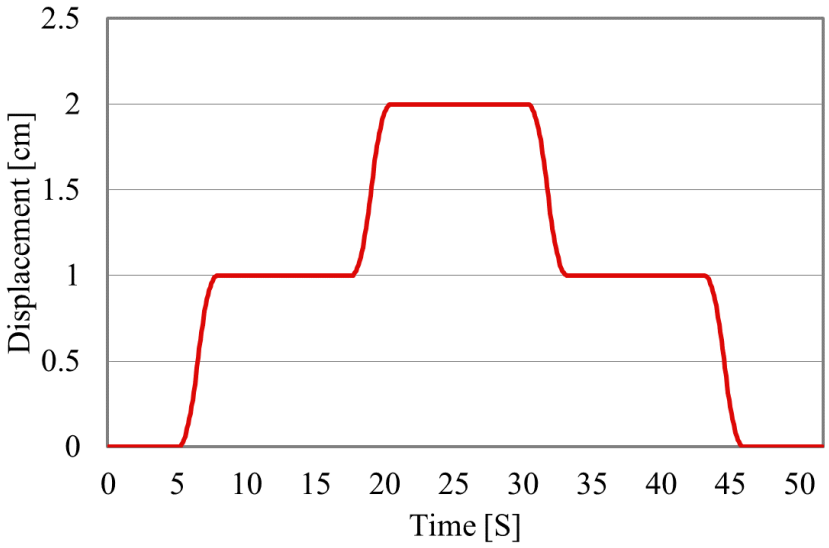

Fig. 35 Step motion

In Fig. 36, the measured results of this step motion are shown. Fig. 37 and Fig. 38 show the IQ plot and arctangent demodulated signals respectively. These results show that the acquired data of the ac coupled system is completely collapsed due to the effect of filtering. On the other hand, the dc coupled system acquired raw data without any distortion and demodulated accurately.

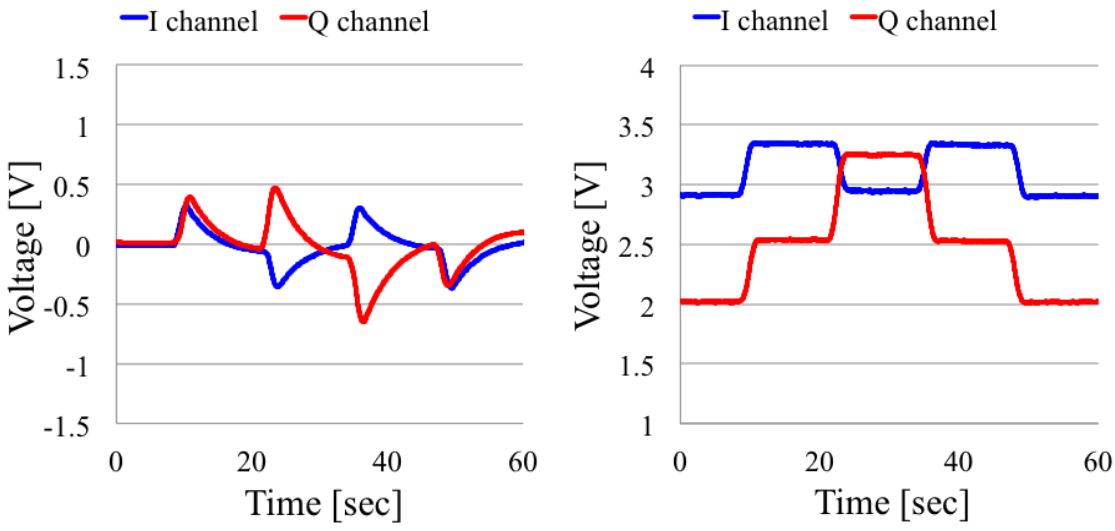

(a) AC coupled (b) DC coupled

Fig. 36 Measured results (Step motion)

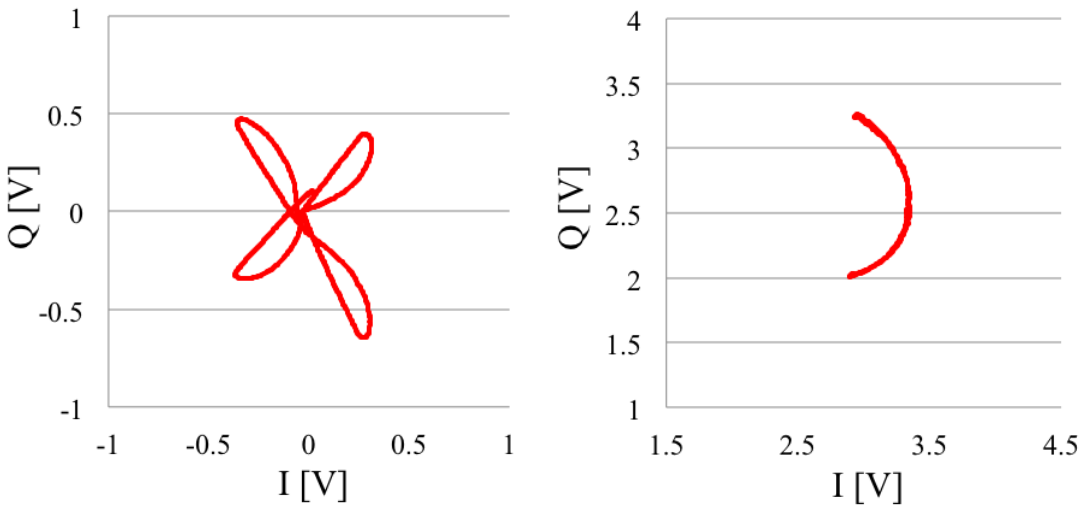

(a) AC coupled (b) DC coupled

Fig. 37 IQ plot

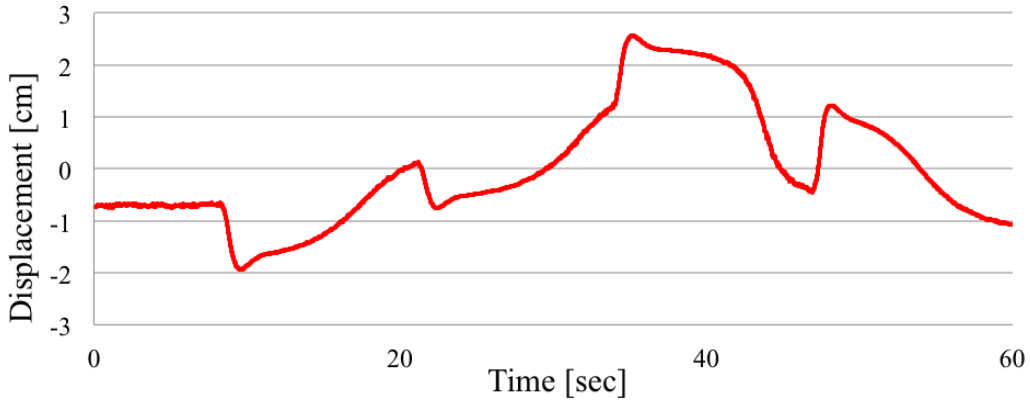

(a) AC coupled

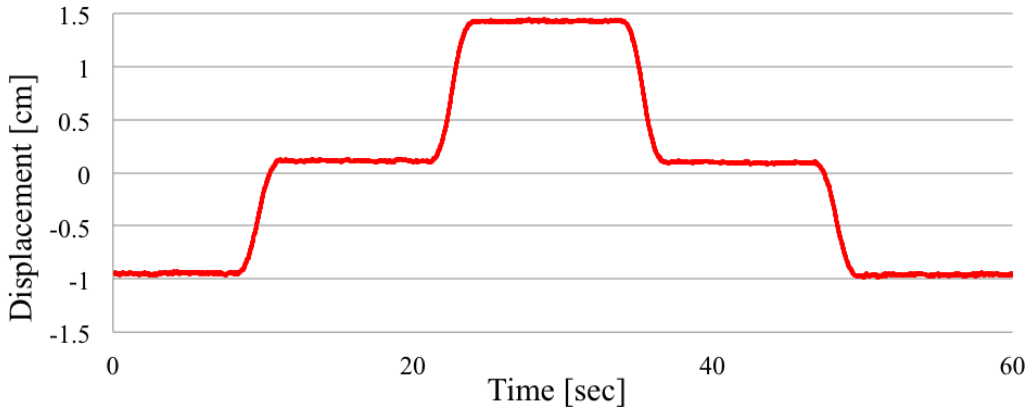

(b) DC coupled

Fig. 38 Arctangent demodulated signal

4.2. RF DC Offset Cancellation

The previous section discusses how the dc offset cancelling is realized by implementing a phase shifter and dc power source. Based on the comparison with the ac coupled system, the proposed dc coupled system can achieve accurate displacement without causing signal distortion and saturation. However, providing an extra dc power source is bothersome. Also the noise on the dc power can be amplified by the differential amplifier so it requires special care for noise. In direct conversion transceiver systems, there are three internal dc offset conditions depending on the magnitude of mixer dc offset and leakage dc offset. In Fig. 39, the three cases are shown. It assumes the leakage signal phase is at 225-degrees so that the mixer dc offset and leakage dc offset vectors are in the opposite direction of each other. For Fig. 39 a), the magnitude of mixer dc offset is larger than the leakage dc offset. In this case, the internal dc offset at 225-degree is always positive and never reaches zero. All the measurements shown in the previous section falls in this category. Thus, the proposed dc offset optimization technique described in the previous section requires a dc power source at the input of the baseband amplifier in order to compensate for the rest of the dc offset from the system. In Fig. 39 b), since the magnitude of the mixer dc offset is smaller than leakage dc offset, the dc offset point at 225-degrees is negative dc offset. This condition also requires dc power source to cancel the rest of dc offset from the system. The third condition is when both magnitude of mixer dc offset and leakage dc offset are the same. In this case, the dc offset at 225-degrees is at the zero dc offset for both I and Q channels. Thus, it can be

cancelled without dc power source at the baseband. Therefore this condition is the ideal case of the internal dc offset.

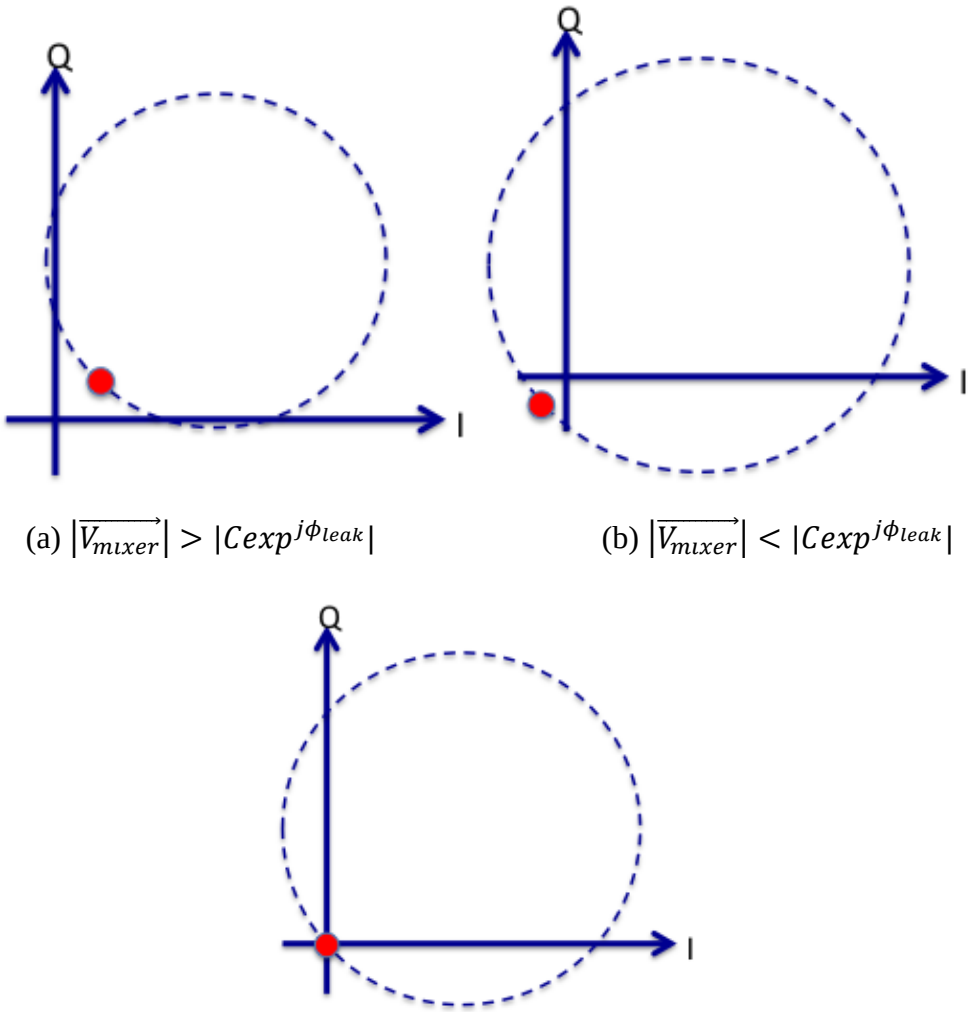

(a) $\left|\overrightarrow{V_{mixer}}\right| > |Cexp^{j\phi_{leak}}|$ (b) $\left|\overrightarrow{V_{mixer}}\right| < |Cexp^{j\phi_{leak}}|$

(c) $\left|\overrightarrow{V_{mixer}}\right| = |Cexp^{j\phi_{leak}}|$

Fig. 39 Three different conditions of internal dc offset

The proposed RF dc offset optimization system block diagram is shown in Fig. 40. Based on the analysis above, in order to achieve the ideal condition, the Tx leakage signal amplitude is adjusted by simply increasing the RF signal source output level while the ideal mixer LO signal level is maintained by the variable attenuator introduced between

first and second power divider in the LO chain. The measured internal dc offset circle with and without dc cancelling is shown in Fig. 41. As described above, without cancelling case, there is some dc offset at 225-degrees on the internal dc offset circle. On the other hand, with cancelling case, the dc offset circle reaches zero. Therefore it is possible to achieve zero dc offset by adjusting the phase of the RF chain.

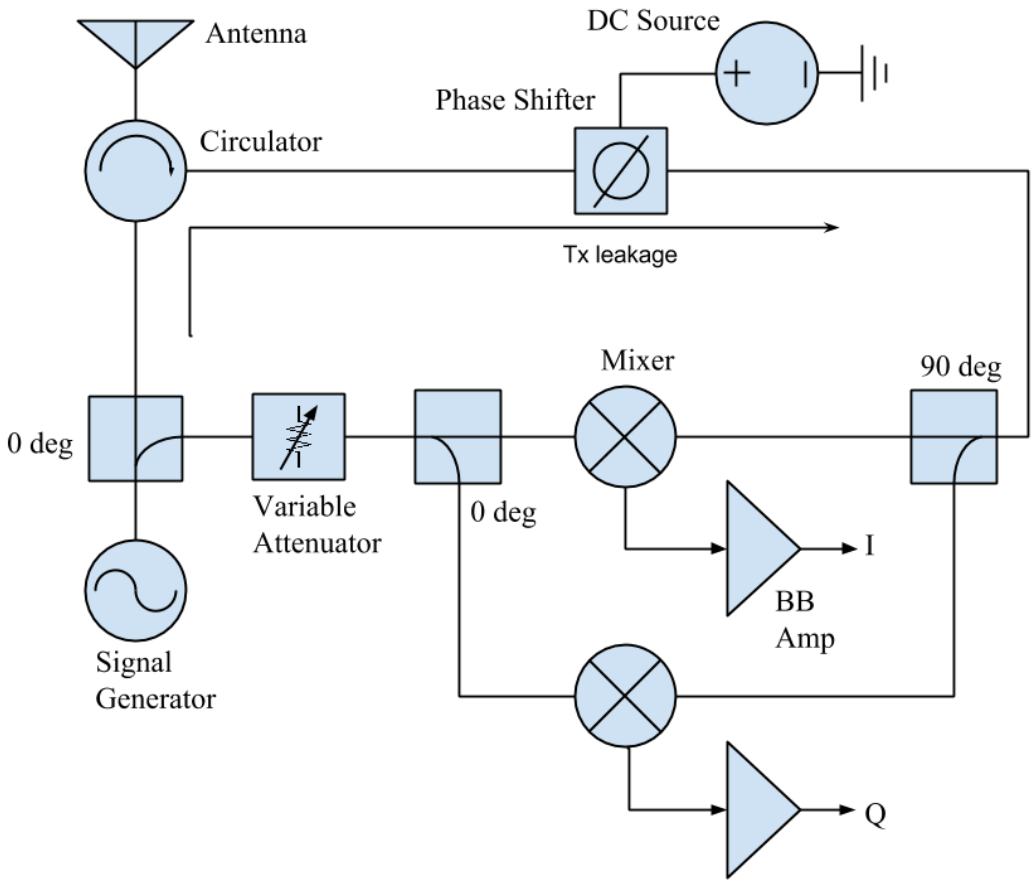

Fig. 40 RF dc cancellation system

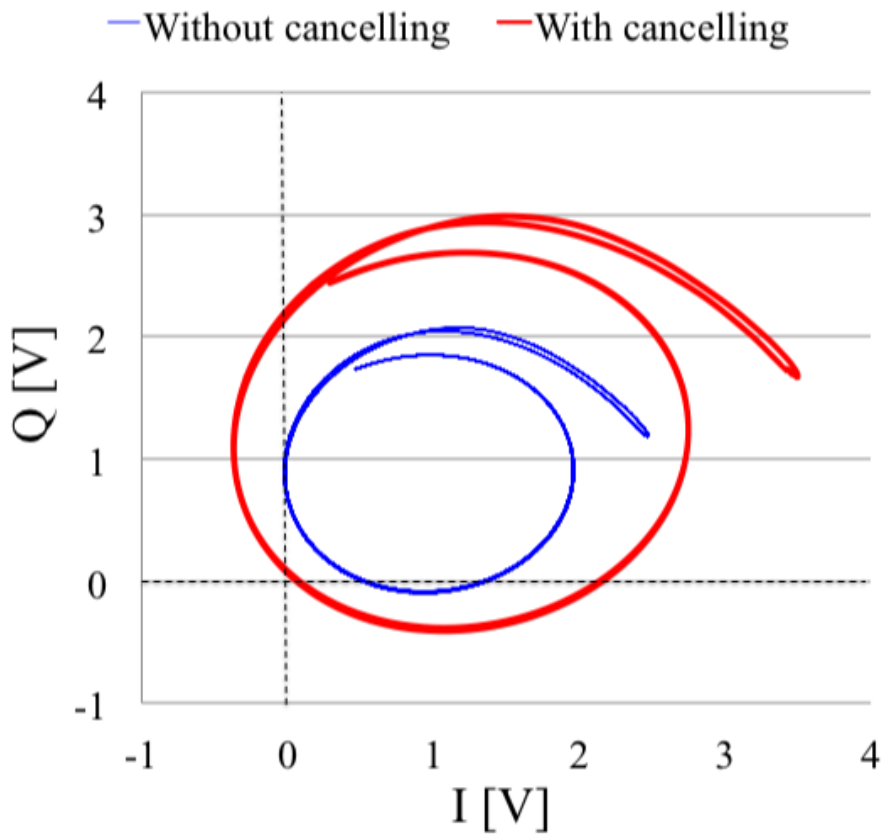

Fig. 41 The internal dc offset circle with[red]/without[blue] dc offset cancelling

With this proposed system, a linear actuator, which moves as sinusoidal motion with 0.2Hz rate with 1 cm displacement, is measured. The radar output signals from I and Q channels are shown in Fig. 42. The IQ plot and the demodulated signal are shown in Fig. 43 and Fig. 44, respectively.

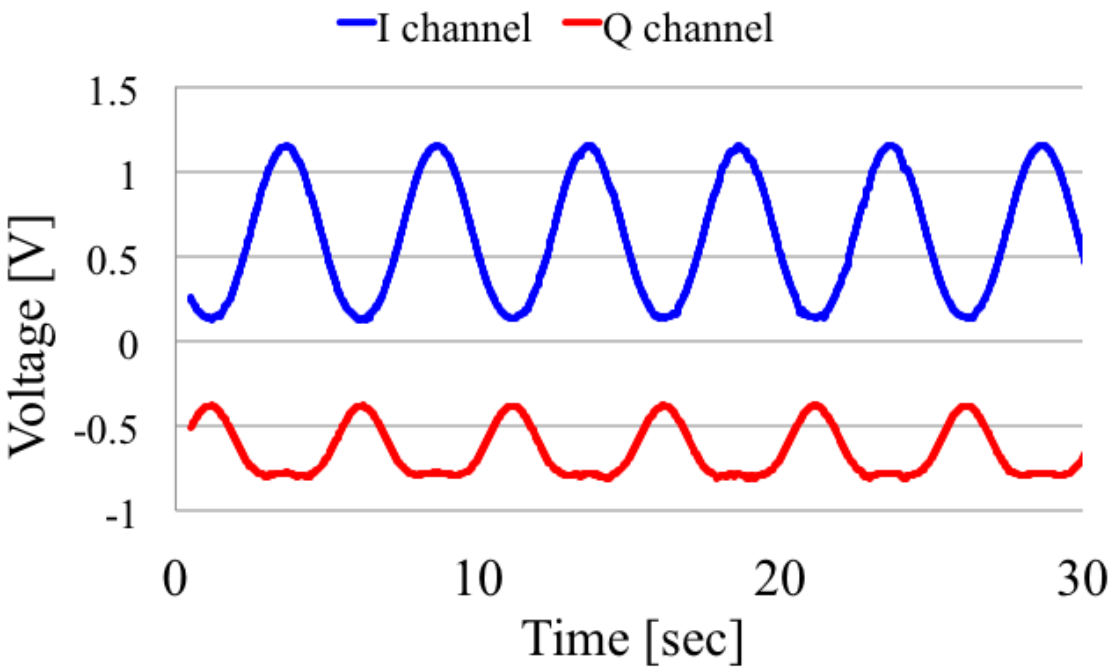

Fig. 42 Radar output data (0.2Hz 1cm displacement)

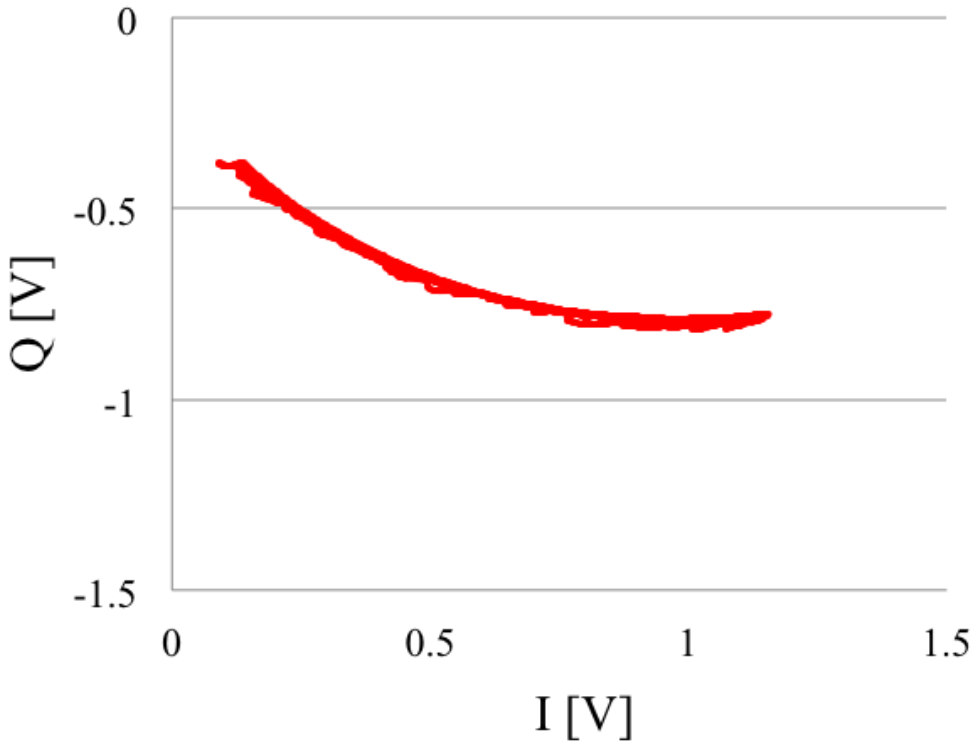

Fig. 43 IQ plot

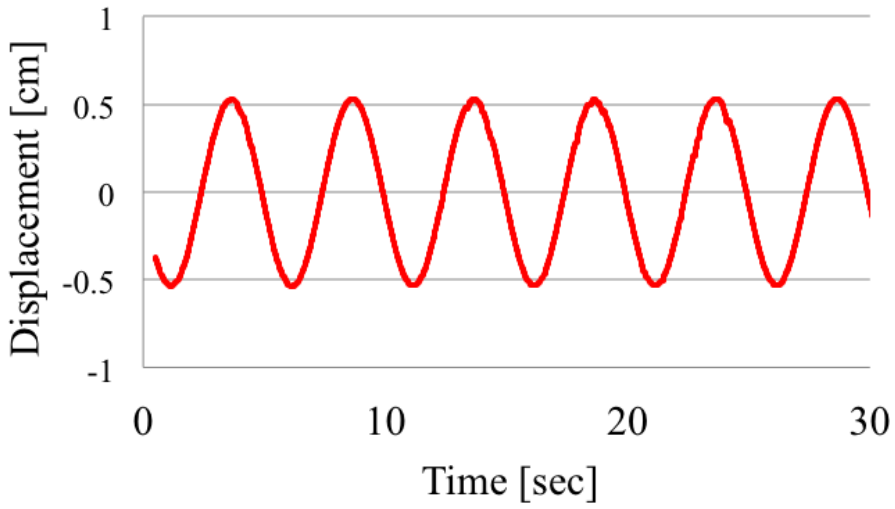

Fig. 44 Demodulated signal

In order to compare these results with another dc offset compensation method, the step motion that was used to demonstrate the effect of the proposed dc compensation method is measured. The raw radar output signals are shown in Fig. 45. The IQ plot and center finding result are shown in Fig. 46, and the demodulated signal is shown in Fig. 47.

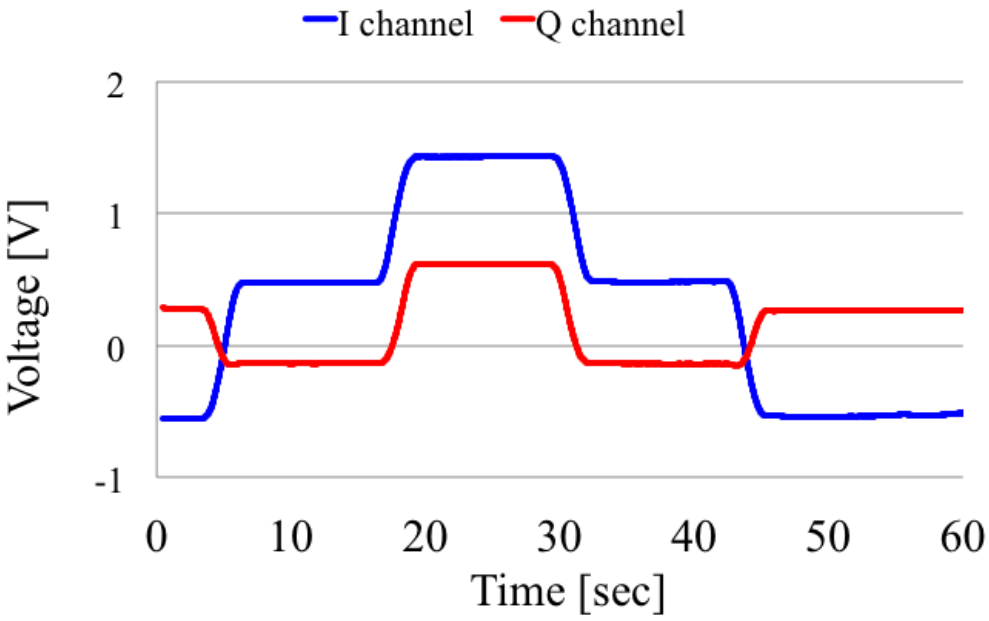

Fig. 45 Radar output signal (Step motion)

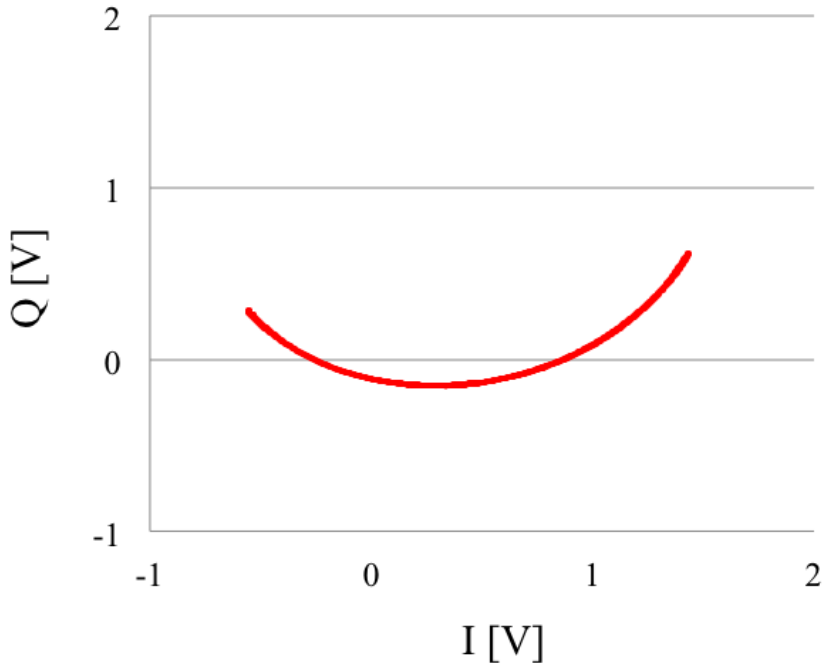

Fig. 46 IQ plot

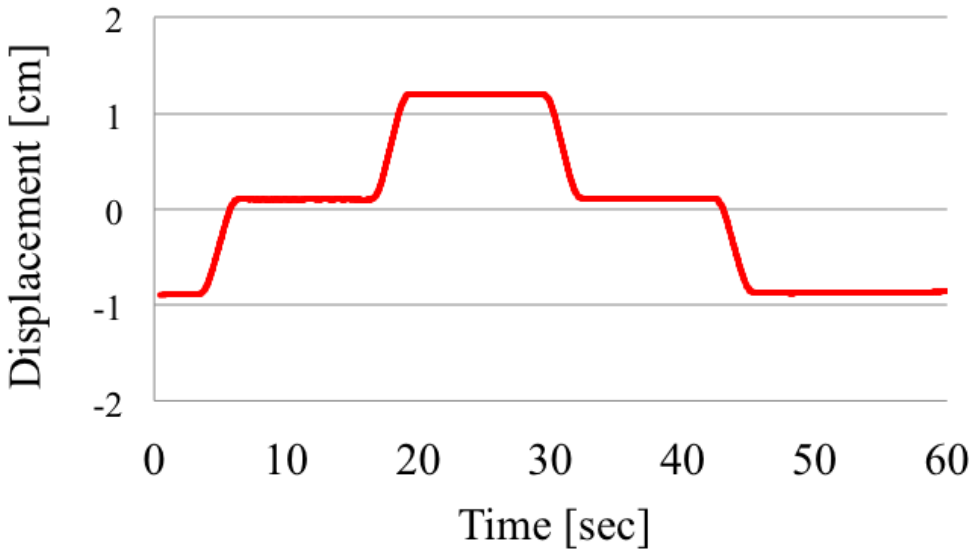

Fig. 47 Demodulated signal

Next, normal breathing of a human subject is measured with this method. In Fig. 48, the raw radar output signals are shown. The IQ plot and center finding result is shown in Fig. 49, and the demodulated signal is shown in Fig. 50. From these results, it is clear that this dc offset compensation technique works very well by cancelling dc offset to achieve a dc coupled system. However, because the arc length caused by the human breathing motion with 2.4GHz system is not sufficient enough, the center finding method does not work well which causes the displacement calculation error, as shown in Fig. 49.

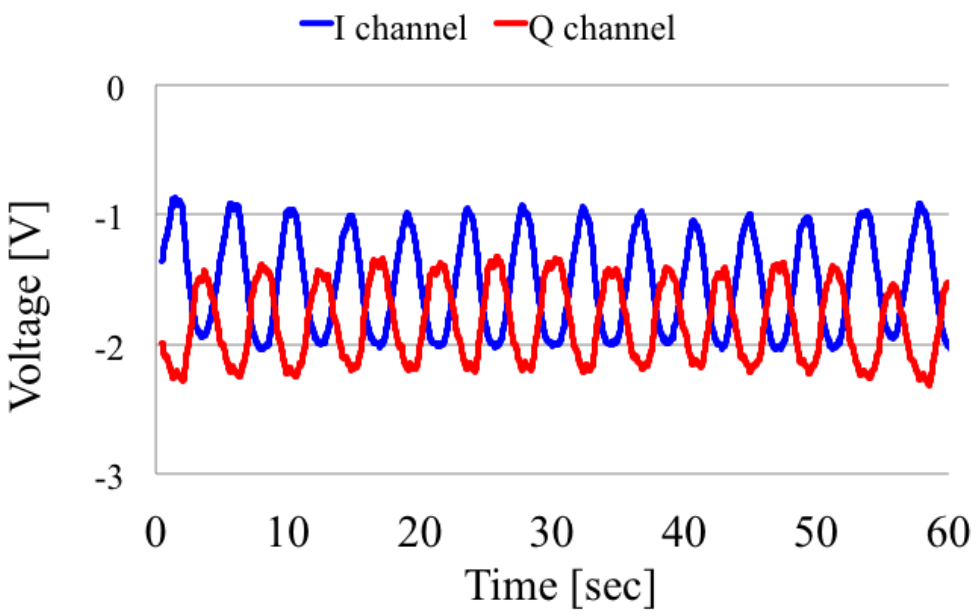

Fig. 48 Radar output signal (Human breathing)

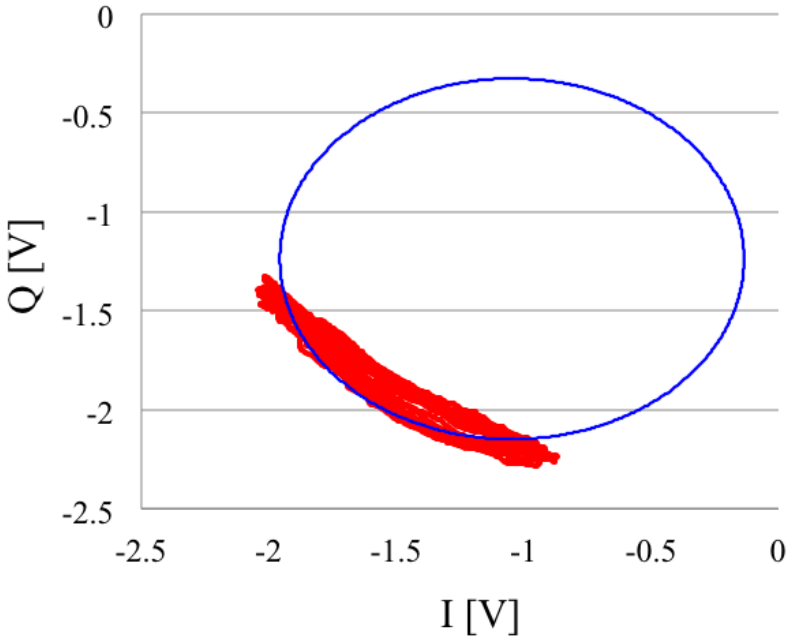

Fig. 49 IQ plot with estimated circle

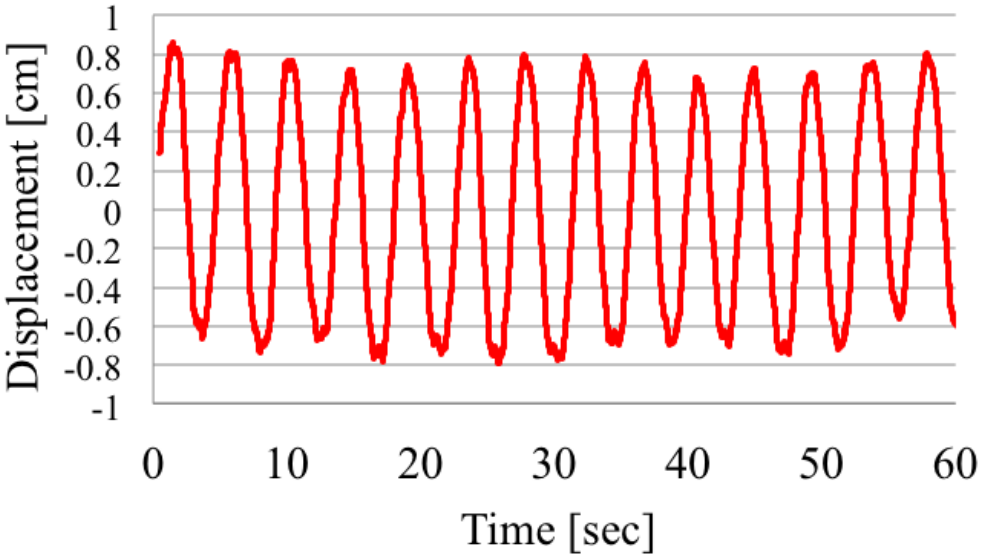

Fig. 50 Demodulated signal

CHAPTER 5

THE RADAR RANGE EQUATION FOR ACCURATE DISPLACEMENT DETECTION

5.1 Frequency and the arc length

Although it is possible to obtain relative displacement information using arctangent demodulation, applying this method to the signal acquired by the direct conversion system is problematic. It requires pre-processing, including removing the unwanted dc offset from the radar output signal without removing the dc information. This signal processing method is known as the center finding methods that have been studied [10-11]. In order to find the center of the circle accurately using this process, it is important to achieve better signal to noise ratio as well as longer arc length on an IQ complex plot created by the motion of the subject. In other words, the center finding method relies on the estimation of the full circle based on the arc; therefore the arc length significantly affects to the accuracy of the signal processing. In Fig. 51, accuracy of the center finding process and the demodulation process is shown. In this calculation, the arctangent demodulation process is applied to an arc on unit circle with dc offset ($V_r + e^{j\theta}$) as the processed data by the center estimation algorithm. This plot shows that it is important to achieve higher accuracy of the center finding process in order to obtain the higher demodulation accuracy.

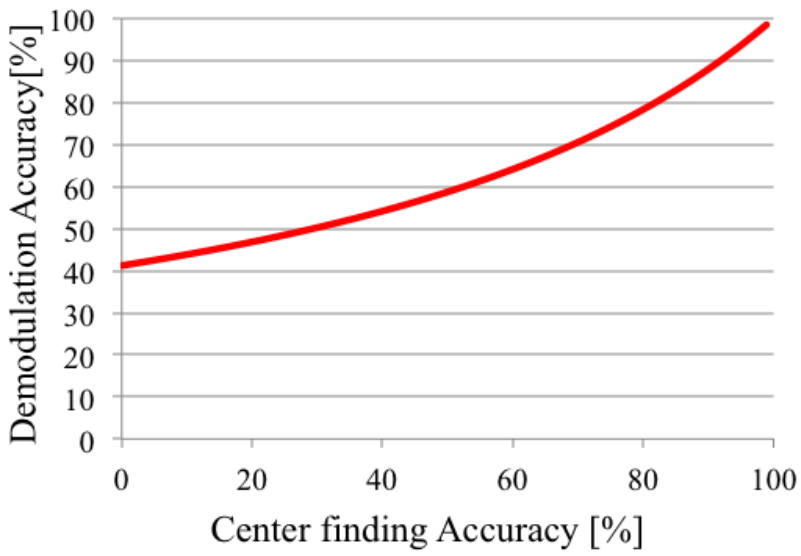

Fig. 51 Accuracy of center finding process and Demodulation process

In Fig. 52, the effect of the arc length and SNR on the accuracy of the center finding process is shown. In this calculation, the center finding method reported in [12] is used and applied to find the actual center point at (0, 0). The accuracy is obtained by calculating the difference between actual and estimated center point. Additive white Gaussian Noise (AWGN) in the communications systems toolbox in MATLAB is used to add noises to the signal with specified SNR. This result clearly indicates that it is important to obtain longer arc length and better SNR to achieve higher accuracy with the center finding process.

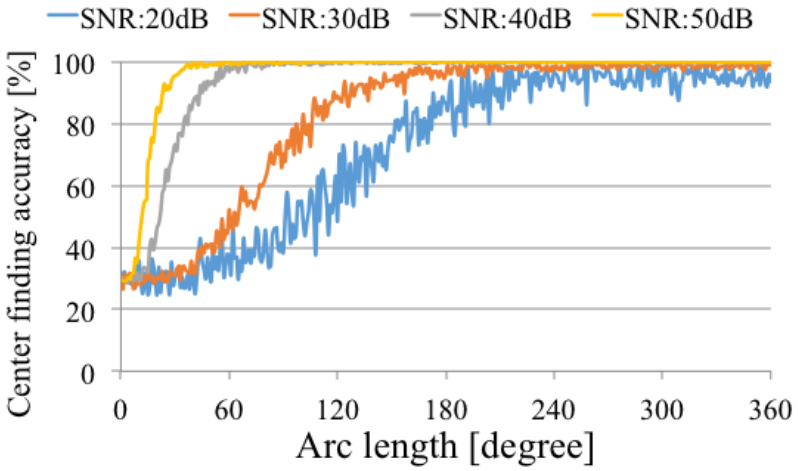

Fig. 52 Center finding accuracy and arc length

The normalized arc length ℓ can be expressed as

$$\ell = 4\pi \frac{D}{\lambda} = 4\pi \frac{Df}{c} \qquad \text{(Eq. 6.1)}$$

where D is the displacement of the moving subject, λ is the wavelength, f is the frequency of carrier signal, and c is the speed of light. From this equation, a system with higher carrier frequency signal achieves longer arc length. However, on the other hand, the one way free space path loss can be expressed as

$$a = \left(\frac{4\pi R}{\lambda}\right)^2 = \left(\frac{4\pi Rf}{c}\right)^2 \qquad \text{(Eq. 6.2)}$$

It is clear that a system with higher carrier frequency suffers an increased free space path loss, so the lower carrier frequency can achieve better SNR. Thus a tradeoff between achieving longer arc length and better SNR exists.

In this chapter, estimation of the SNR and accuracy of center finding method for accurate displacement detection using CW direct conversion Doppler radar is described. In order to estimate the SNR, the well-known radar range equation is extended and applied to this technology.

5.2 Range Equation for Displacement Detection

In this section, the derivation of the extended radar range equation to identify optimal frequency and the system for accurate displacement detection using CW Doppler radar is described. In Fig. 53, the block diagram of the quadrature direct conversion system is shown. All the equations described in this paper are based on this system configuration.

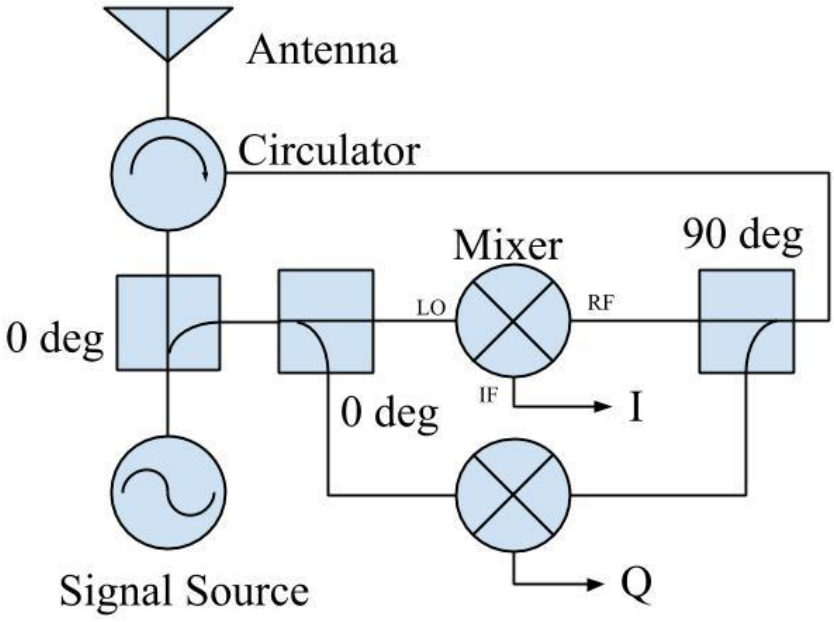

Fig. 53 Block diagram of quadrature direct conversion system

The LO signal at the LO port of the mixer is expressed as

$$V_{LO}(t) = A_{LO}\cos(\omega t) \qquad \text{(Eq. 6.3)}$$

Likewise, the RF port input signal can be expressed as

$$V_{RF}(t) = A_{RF}\cos(\omega t + \theta + p(t)) \qquad \text{(Eq. 6.4)}$$

where θ is the constant phase shift depending on the distance between radar and subject. The received signal strength at the antenna P_r can be expressed by well-known radar range equation

$$P_r = \frac{P_s G^2 \sigma \lambda^2}{(4\pi)^3 R^4} \quad \text{(Eq. 6.5)}$$

where P_s is the transmitted signal power at the antenna, G is the antenna gain, σ is the radar cross-section, λ is the wavelength of carrier signal, and R is the distance between radar and subject. Also the noise floor at the RF frequency band is

$$N_o = kTBF \quad \text{(Eq. 6.6)}$$

where k is Boltzmann constant, T is the temperature in Kelvin, B is the receiver noise bandwidth, and F is the noise figure. Using those two equations, the signal to noise ratio at RF band is expressed as

$$SNR_{rf} = \frac{P_r}{N_o} = \frac{P_s G^2 \sigma \lambda^2}{(4\pi)^3 R^4 kTBF} \quad \text{(Eq. 6.7)}$$

For human vital signs detection using this technology, the required bandwidth is very narrow, such as less than few hundred hertz. Thus the noise floor at the RF band can be expected to be very low. In other words, SNR at the RF band is not the dominant factor of the system sensitivity.

The received signal is split by a 90-degree power splitter to obtain quadrature signal; thus the input signal power of the RF port of mixer is half:

$$P_{rf} = \frac{P_r}{2} \quad \text{(Eq. 6.8)}$$

Assuming the signal is a sinusoidal wave, the peak amplitude of this signal in voltage can be expressed as

$$V_{RF\_peak} = \sqrt{2 P_{rf} Z_0} = \sqrt{\frac{P_s G^2 \sigma \lambda^2 Z_0}{(4\pi)^3 R^4}} = A_{RF} \quad \text{(Eq. 6.9)}$$

where Z_0 is characteristics impedance. Assuming there is no loss in the receiver chain,

this peak voltage is equal to A_{RF}. Thus, the equation of the signal at the RF port of mixer can be rewritten as

$$V_{RF} = A_{RF}\cos(\omega t + \theta + p(t)) = \sqrt{\frac{P_s G^2 \lambda^2 Z_0}{(4\pi)^3 R^4}}\cos(\omega t + \theta + p(t)) \qquad \text{(Eq. 6.10)}$$

The mixer output signal can be expressed as

$$\begin{aligned} V_{bb}(t) &= k\{V_{LO}(t) \times V_{RF}(t)\} \\ &= \frac{kA_{LO}A_{RF}}{2}\{\cos(\theta + p(t)) + \cos(2\omega t + \theta + p(t))\} \\ &= G_c A_{RF}\{\cos(\theta + p(t)) + \cos(2\omega t + \theta + p(t))\} \end{aligned} \qquad \text{(Eq. 6.11)}$$

where k is the mixer conversion factor and G_c is the conversion gain/loss. After low pass filter, this equation can be expressed as

$$V_{bb}(t) = G_c A_{RF}\cos(\theta + p(t)) = A_{bb}\cos(\theta + p(t)) \qquad \text{(Eq. 6.12)}$$

Based on this equation, in the quadrature system, the dc offset is calculated as

$$V_{dc} = \sqrt{(A_{bb}\cos\theta)^2 + (A_{bb}\sin\theta)^2} = A_{bb} \qquad \text{(Eq. 6.13)}$$

Assuming there is no clutter and system internal dc offset, this dc offset is created by the subject. Therefore, it represents the dc information, which is the vital information for arctangent demodulation [4]. Based on these equations, the 1cm displacement of a 15 x 20 [cm] flat metal plate at 1m distances is calculated and measured. The results on the complex IQ plot are shown in Fig. 54. The parameters for this measurement and calculation are: Distance R: 1[m], RCS σ: 0.41 [18], Displacement: 1 [cm], Carrier signal frequency: 2.4 [GHz], RF output power: 10[dBm], LO signal power: 7[dBm], Antenna gain: 8[dB], Mixer conversion loss: 6[dB], and Baseband amplifier gain: 60[dB]. This plot shows good agreement between calculated and measured IQ plots.

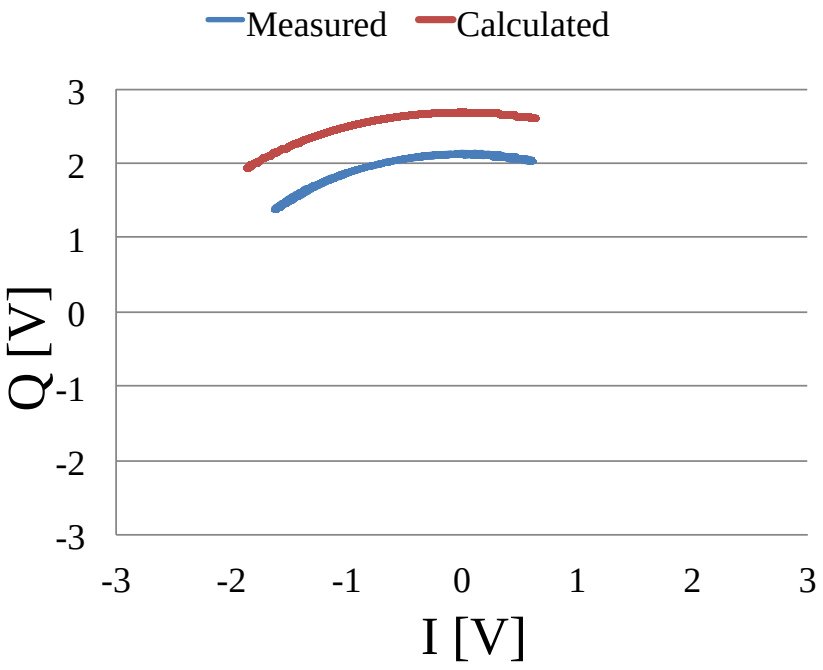

Fig. 54 Measured and calculated IQ plot

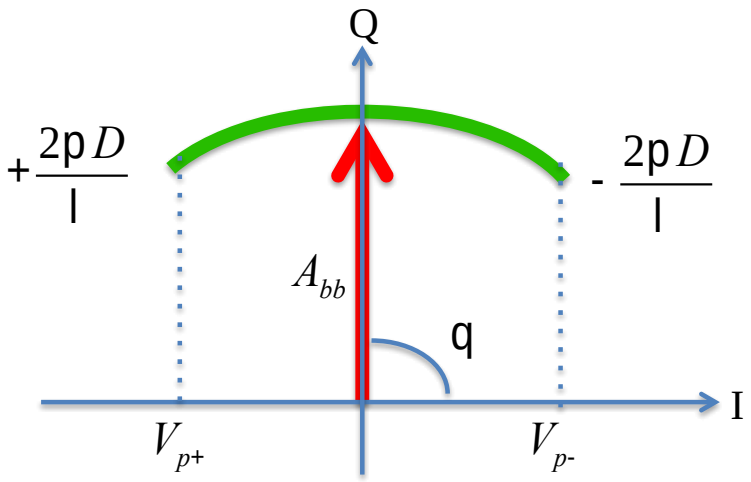

Fig. 55 Image of peak-to-peak value of signal

In order to estimate the signal to noise ratio at baseband, the RMS voltage of the baseband signal is required. In Fig. 55, an image of peak-to-peak value calculation is shown. Based on this, the peak-to-peak amplitude of baseband signal can be calculated as

$$V_{pp} = A_{bb}\left\{\cos\left(q+\frac{2pD}{l}\right) - \cos\left(q+\frac{2pD}{l}\right)\right\} \quad \text{(Eq. 6.14)}$$

In addition, depending on the angle θ and the arc length ℓ, the amplitude of the signal is varied ($V_{pp}(\theta, \ell)$). In paper [9], with respect to the θ of radar output signal, two extreme cases for I and Q channels, optimum and null, are described. In the same manner, the signal amplitude of the two extreme cases are:

i) Optimum case

$$V_{pp\_opt}(\ell) = \begin{cases} 2A_{bb}\sin\left(\frac{2pD}{l}\right), & \ell < p \\ 2A_{bb}, & p \le \ell \end{cases} \quad \text{(Eq. 6.15)}$$

ii) Null case

$$V_{pp\_null}(\ell) = \begin{cases} A_{bb}\left\{1 - \cos\left(\frac{2pD}{l}\right)\right\}, & \ell < 2p \\ 2A_{bb}, & 2p < \ell \end{cases} \quad \text{(Eq. 6.16)}$$

In addition to those two cases, another important case is when θ is at 45-degree. At this angle, the signal amplitude of both I and Q channels are identical. In all other angles, the signal amplitude of one of the IQ channel is always larger than this case. Therefore, this angle, $\theta = 45°$, can be assumed as the minimum SNR case. The signal amplitude can be expressed as

$$V_{pp\_45^\circ}(\ell)=\begin{cases}\sqrt{2}A_{bb}\sin\left(\dfrac{2\pi D}{l}\right), & \ell<\dfrac{\pi}{2}\\ A_{bb}\left[1-\dfrac{\sqrt{2}}{2}\left\{\cos\left(\dfrac{2\pi D}{l}\right)-\sin\left(\dfrac{2\pi D}{l}\right)\right\}\right], & \dfrac{\pi}{2}\le\ell\le\dfrac{3}{4}\pi\\ 2A_{bb}, & \dfrac{3}{4}\pi\le\ell\end{cases} \quad \text{(Eq. 6.17)}$$

With these equations, the normalized amplitude of baseband signal and arc length with respect to three different cases is shown in Fig. 56. Based on this plot, when arc length becomes half circle (180-degrees), the optimum case reaches the maximum amplitude ($2A_{bb}$). On the other hand, the null case signal amplitude does not reach the maximum amplitude until the arc becomes full circle (360-degrees). In addition, the $\theta = 45°$ case reaches the maximum amplitude at 270-degrees when the arc becomes 3/4 of a full circle. At any angle θ with this arc length, either one channel or both channels will achieve maximum amplitude. Achieving a longer arc than this length does not improve the SNR. Therefore, this arc length can be assumed as the longest useful arc. In other words, if the estimated arc length with the carrier frequency is longer than this length, the system may only suffer more free space losses.

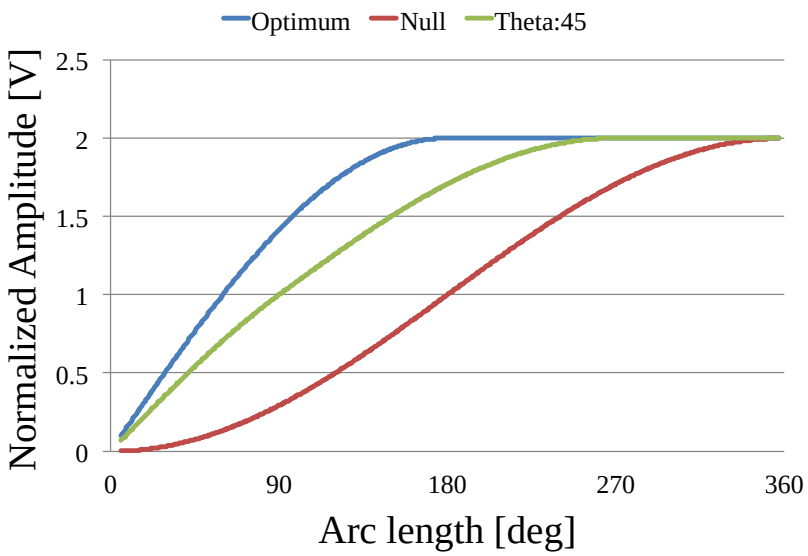

Fig. 56 Normalized amplitude of baseband signal and arc length

Assuming the signal is sinusoidal, the baseband signal in RMS voltage can be expressed as

$$V_{rms} = \frac{\sqrt{2}}{2} V_{pp} \qquad \text{(Eq. 6.18)}$$

Based on this equation, baseband signal level caused by human breathing motion is calculated with respect to frequency and shown in Fig. 57. The parameters for this calculation are: Distance R: 1[m], RCSσ: 0.08 [19], Displacement: 1 [cm], Carrier signal frequency: 2.4 [GHz], RF output power: 10[dBm], LO signal power: 7[dBm], Antenna gain: 8[dB], Mixer conversion loss: 6[dB]. Since higher frequency suffers more free space loss, signal level is degraded at a higher frequency. The arc created by this motion becomes full circle at 15GHz; thus the baseband signal become independent from the angle θ at this frequency. The arc becomes 3/4 of circle at 11GHz; thus the available highest frequency can be assumed as 11GHz, as described above.

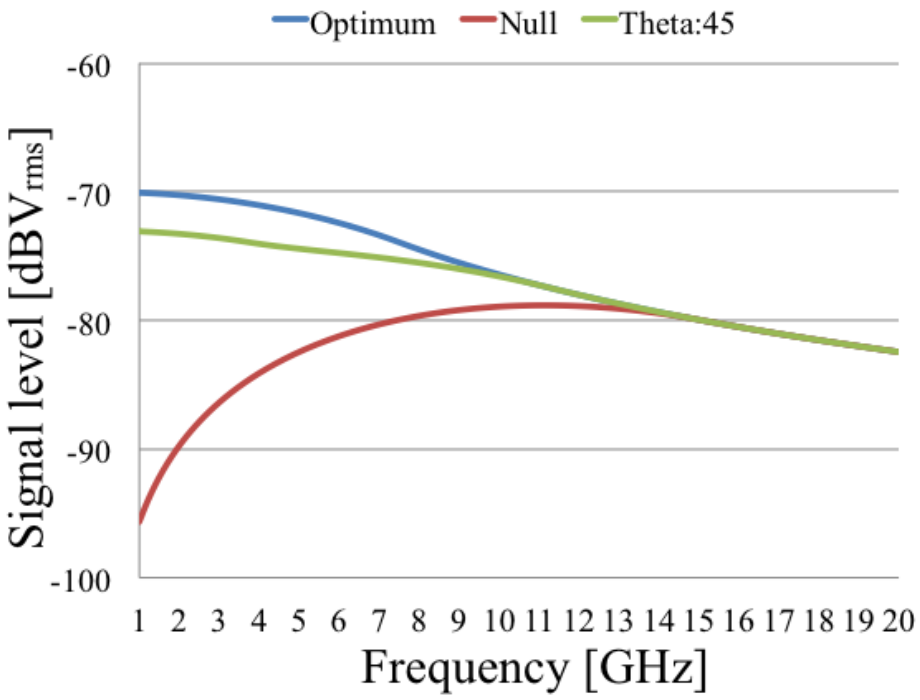

Fig. 57 Baseband signal level and frequency

Based on paper [13-16], due to flicker noise, the noise floor at the baseband frequency is much higher than the RF band noise floor described above. The general flicker noise model can be expressed as

$$N_{o\_bb} = n\sqrt{\frac{f_c B}{f}} \qquad \text{(Eq. 6.19)}$$

where n is the noise density level, f_c is the corner frequency of flicker noise, and B is the bandwidth [17]. The measured flicker noise at a mixer output port is shown in Fig. 58.

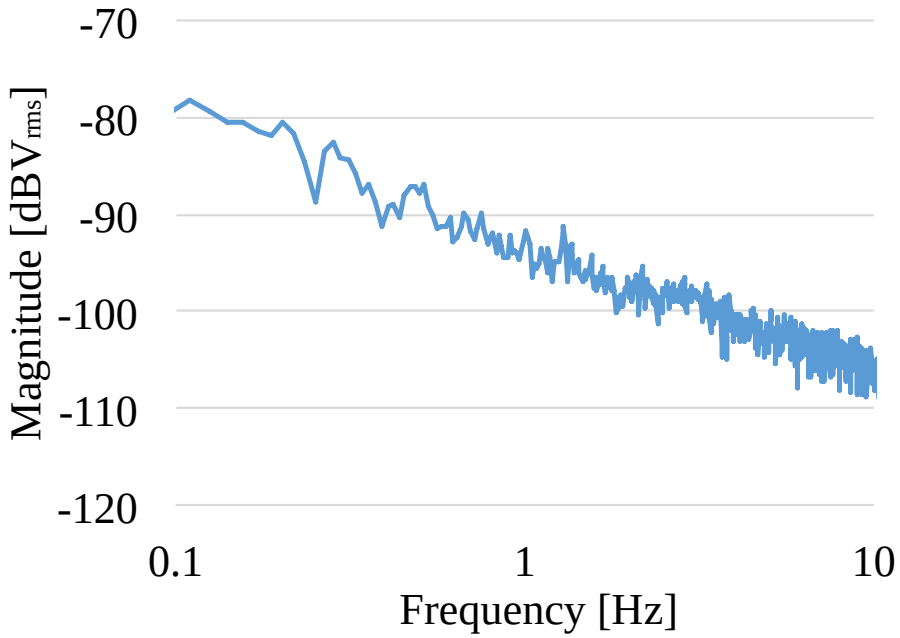

Fig. 58 Measured flicker noise at a mixer output

Using equation for baseband signal and the noise floor, the signal to noise ratio at mixer output is expressed as

$$SNR_{bb} = \frac{V_{bb\_rms}}{N_{o\_bb}} = \frac{V_{pp}\sqrt{f}}{2n\sqrt{2f_cB}} \quad \text{(Eq. 6.20)}$$

Also, the minimum baseband signal V_{bb_min} can be expressed as

$$V_{bb\_\min} = N_{o\_bb} \times SNR_{bb\_\min} \quad \text{(Eq. 6.21)}$$

where SNR_{bb_min} is the minimum SNR required at baseband. Based on the equations derived, the circle fitting accuracy and baseband signal level respect to frequency with (a)10mm and (b)5mm displacement is shown in Fig. 59.

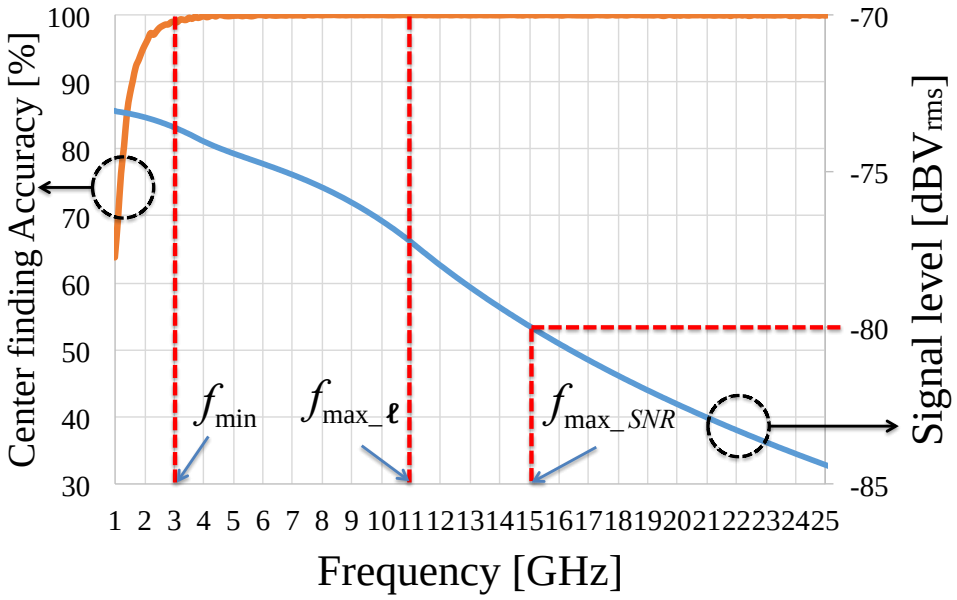

(a) D = 10 mm

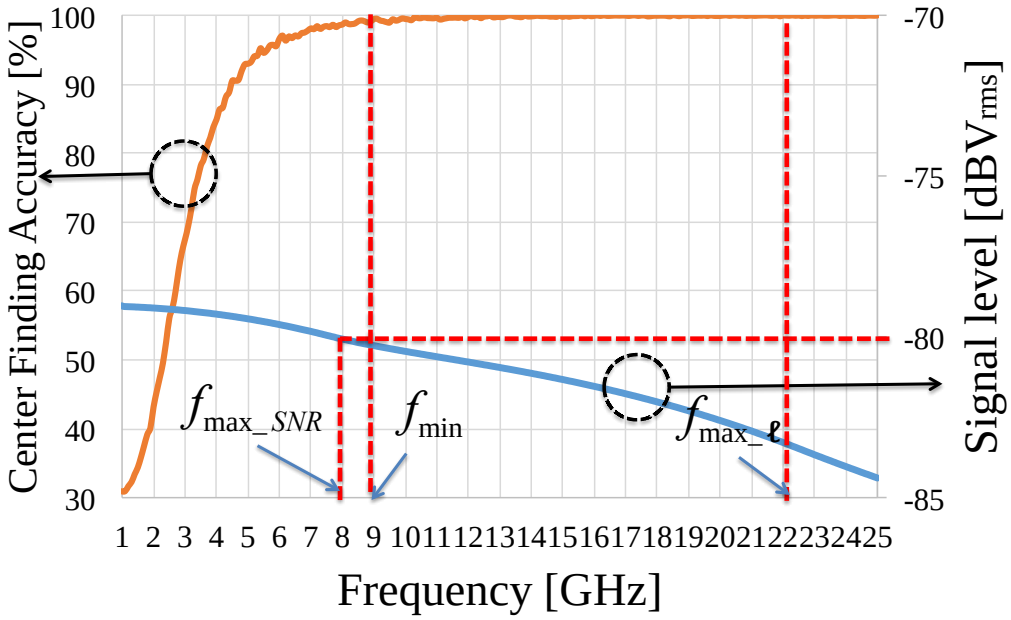

(b) D = 5mm

Fig. 59 Center finding accuracy, baseband signal level and frequency

The signal level shown in this plot is at the output of mixer before applying the

amplification since the SNR is expected to be the lowest at the point in the system. On the other hand, the center finding accuracy is calculated based on the 35dB of SNR improvement after taking into account the 60dB of gain with 25dB of noise figure in baseband.

First, the lowest frequency (f_{min}) can be found by the center finding accuracy at which reaches enough accuracy. Based on the plots, about 3GHz for 10mm and 9GHz for 5mm displacement. In comparison with these two cases, since the displacement becomes half, higher frequency is required to achieve an accurate center finding process.

Next, the highest frequency can be found by the signal level plot. At the frequency ($f_{\max\_SNR}$), the signal level reaches the noise floor shown in Fig. 58. Thus, any higher frequency than this cannot detect the motion. Based on the plots, about 15GHz for 10mm and 8GHz for 5mm displacement.

In addition, the arc length reaches to 3/4 of circle at frequency ($f_{\max\_\ell}$). As described above, there is no advantage to use any higher frequency than this frequency unless the system can achieve better SNR with implementing higher gain. Based on the plots, about 11GHz for 10mm and 22GHz for 5mm displacement. In order to detect the displacement accurately, any frequency in between f_{min} and $f_{\max\_SNR}$ can be used as long as the f_{min} is lower than $f_{\max\_SNR}$. Thus, in these two displacements, 5mm displacement cannot be detected by the system and requires improvement of the SNR.

In same manner using those equations, with a fixed frequency at 2.4GHz, the demodulation accuracy with 10mm displacement respect to various distance, and 1m distance respects to various displacement are shown in Fig. 60 and Fig. 61 respectively. Based on those plots, the maximum distance to detect 10mm displacement is less than

1m, and the smallest detectable displacement at 1m is about 11 mm with the 2.4GHz system. Displacements smaller than this still can be seen; however the displacement cannot be detected accurately due to the center finding error.

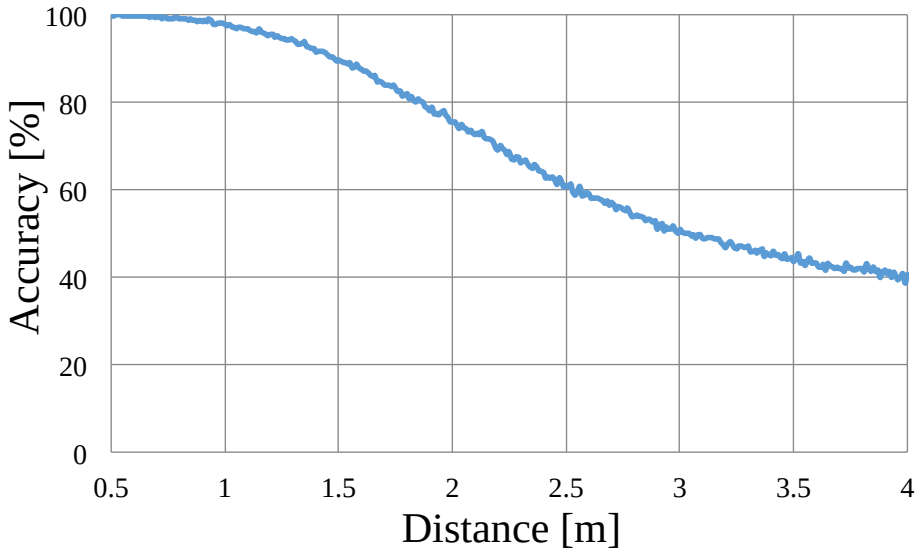

Fig. 60 Demodulation accuracy and distance

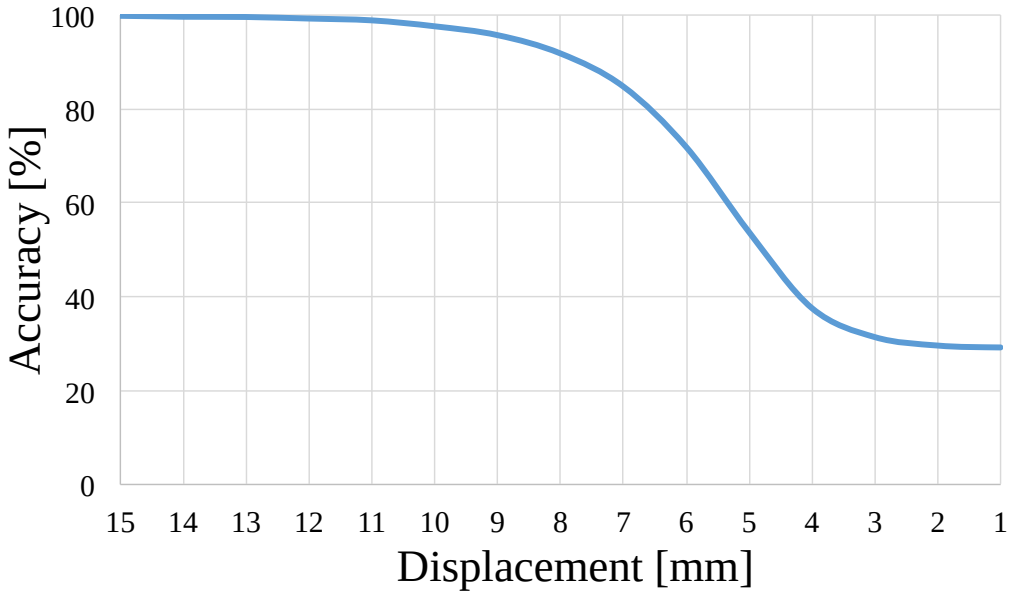

Fig. 61 Demodulation accuracy and displacement

5.3 Human breathing measurement

Based on the calculation results shown in Fig. 59, in order to detect human breathing accurately, which is assumed at about 10mm displacement [6], the 2.4GHz is not suitable and cannot achieve long enough arc length for the center finding process. In order to address this, human breathing is measured using a 2.4 and 5.8 GHz quadrature direct conversion Doppler radar system. The measured IQ plot and the demodulated signal of 2.4 and 5.8 GHz systems are shown in Fig. 62 and Fig. 63 respectively. From Fig. 62(a), the calculated arc length with 10mm displacement at 2.4GHz is about 57.6-degrees; however the fitted circle shows about 90-degrees of arc length. Thus, the center finding process does not work well for this measured result. On the other hand, Fig. 63(a) shows that the arc length based on the fitted circle is about 135-degrees, while the estimated arc length with 5.8GHz is about 139.2-degrees. Therefore it shows good agreement between estimated and measured. The displacement detected with this measurement is about 8mm. These results prove that 2.4GHz system cannot achieve accurate displacement of human breathing due to the center finding error, and also the good agreement with the proposed optimal frequency estimation process based on the equations described in this chapter.

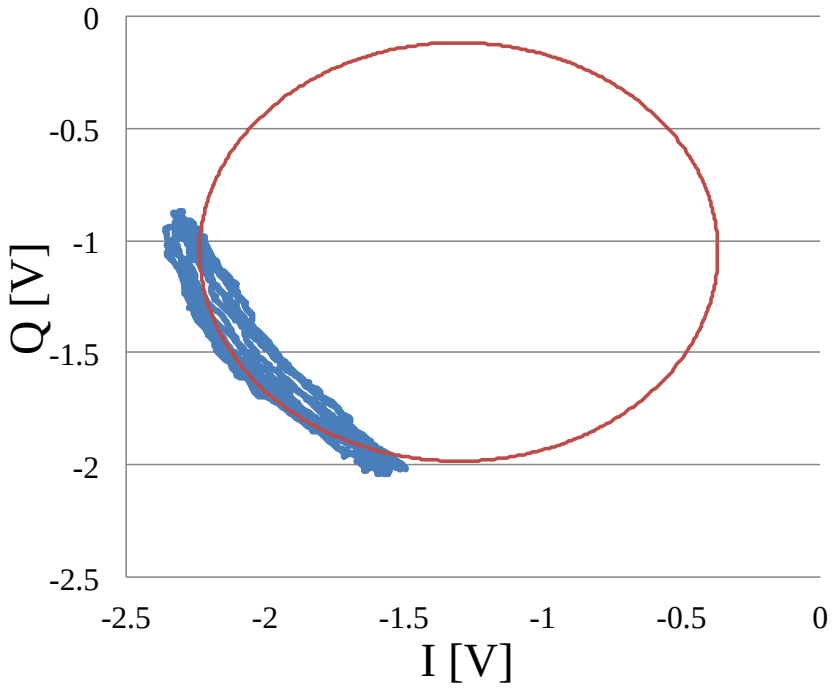

(a) IQ plot

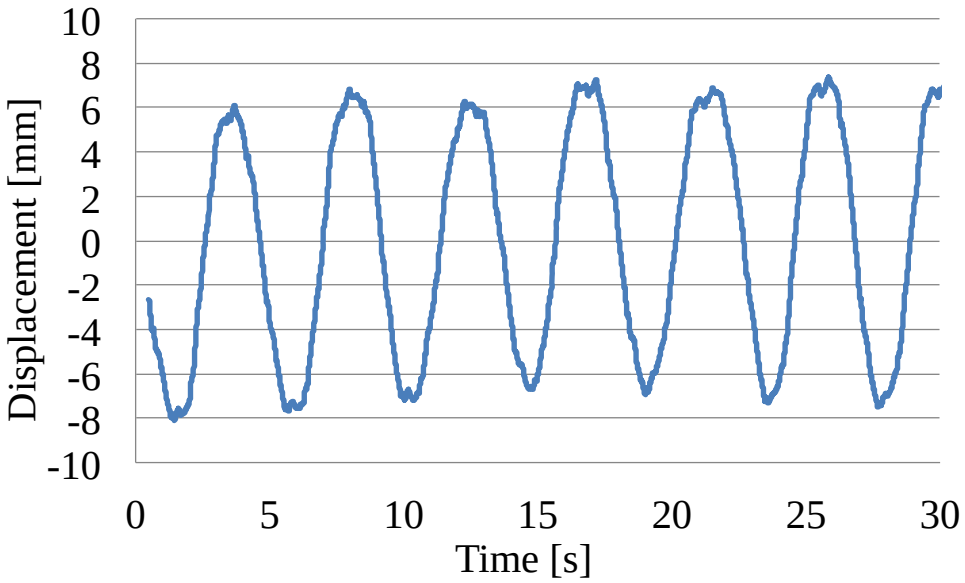

(b) Demodulated signal

Fig. 62 Measured human breathing with 2.4GHz system

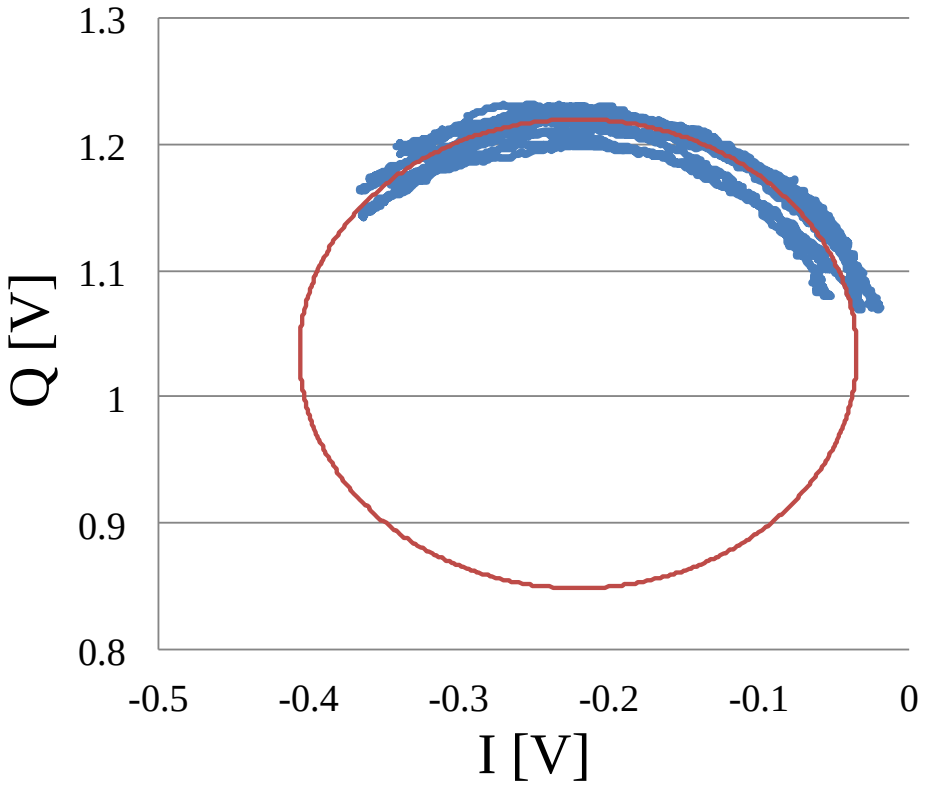

(a) IQ plot

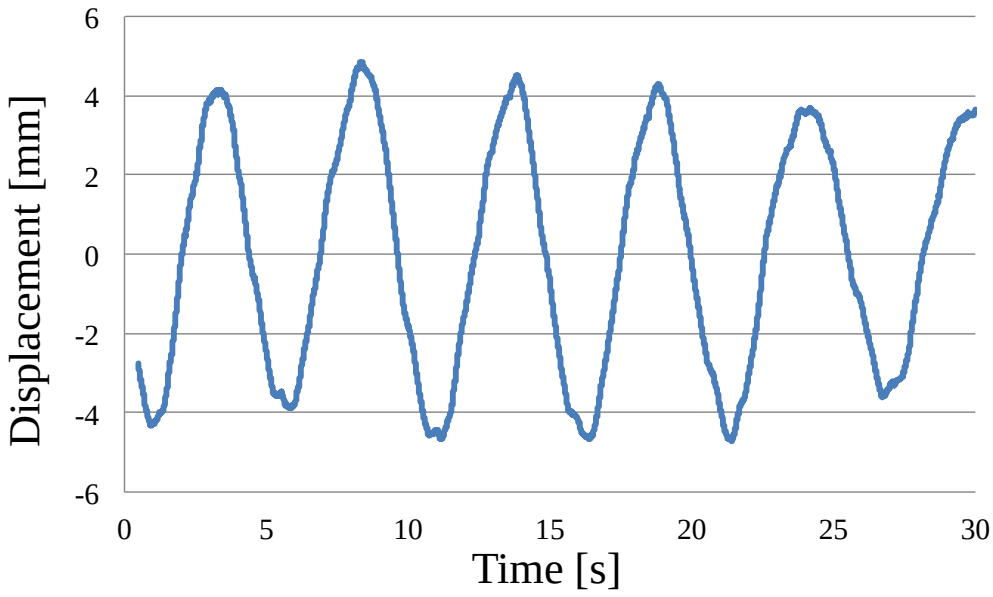

(b) Demodulated signal

Fig. 63 Measured human breathing with 5.8GHz system

CHAPTER 6
CONCLUSION

Accurate displacement detection using RF Doppler radar is studied. Due to its simple structure and validity, direct conversion systems are commonly used for vital sign detection applications. One problem with such systems is that the motion or displacement measurement accuracy is often compromised by the presence of dc offset which limits the overall signal to noise ratio (SNR) and the system resolution.

The dc offset in the direct conversion system is studied and analyzed in depth in chapter 3. While the portion of dc offset caused by system imperfections, internal dc offset, and the external environment, clutter, is problematic, the dc offset contributed from the subject is critical for accurate displacement measurement. The thorough analysis of the dc offset shows that the majority of the dc offset is caused by a system imperfection, which is caused by the mixer and Tx leakage signal. In addition, the dc offset caused by system imperfection is constant dc offset while the clutter dc offset and dc information vary based on the measurement situation and environment.

In chapter 4, the dc offset optimization method of quadrature direct conversion system is described. Based on the analysis in the previous chapter, the dc offset caused by the system imperfection is identified as the major component of the dc offset. Since it is constant, by implementing a phase shifter and dc power source, the internal dc offset optimization can be realized, and therefore a dc coupled system with a decent amount of baseband gain becomes practicable. The measured results confirm that the proposed systems can achieve accurate demodulation results without causing any signal saturation

and signal distortion due to band pass filter, as compared to conventional ac coupling system.

In chapter 5, the estimation of the SNR and accuracy of center finding process for accurate displacement detection is described. In this technology, there is a tradeoff between achieving better SNR and longer arc length, which results in better demodulation accuracy. The SNR mostly depends on free space losses which higher frequency suffers more so the lower carrier frequency can achieve better SNR. On the other hand, the center finding process relies on a circle estimated from the arc. Thus the longer arc results in better center finding process accuracy. In order to achieve a longer arc, higher carrier frequency is required. Therefore, a tradeoff between achieving better SNR and longer arc exists. In order to estimate the optimal carrier frequency and system, the well-known radar range equation is extended to estimate the SNR of this technology. Using the calculated SNR, the accuracy of center finding process is estimated. Based on the SNR and the accuracy of center finding process, the lowest and highest frequency can be estimated. In addition, human breathing is measured with 2.4 and 5.8 GHz systems in order to assess the proposed method. With 2.4 GHz systems, the achieved arc length is not long enough to obtain the center point accurately; thus it results in the inaccurate demodulation. On the other hand, the 5.8GHz system can achieve longer arc length with enough SNR that results in an accurate center finding and demodulation processes. Using the proposed system assessment approach, the system at optimal frequency can be estimated which results accurate displacement detection.

References

[1] A. D. Droitcour, V. M. Lubecke, J. Lin, and O. Boric-Lubecke, “A Microwave Radio for Doppler Radar Sensing of Vital Signs,” IEEE MTT-S International Microwave Symposium, Phoenix, AZ, USA, vol. 1, pp. 175178, May 2001.

[2] A. D. Droitcour, O. Boric-Lubecke, V. M. Lubecke, J. Lin and G. T. Kovacs, “Range Correlation and I/Q Performance Benefits in Single Chip Silicon Doppler Radars for Non-Contact Cardiopulmonary Monitoring” IEEE Trans. on Microwave Theory and Tech., Vol. 52, No. 3, pp. 838-848, March 2004.

[3] S. Yamada, and V.M. Lubecke, “Sub-μW Signal Power Doppler Radar Heart Rate Detection,” Asia Pacific Microwave Conference, Yokohama, Japan, December 2006

[4] B. Park, O. Boric-Lubecke, V. M. Lubecke, “Arctangent Demodulation With DC offset Compensation in Quadrature Doppler Radar Receiver Systems” IEEE Trans. on Microwave Theory and Tech., Vol. 55, No. 5, pp. 1073-1079, May2007.

[5] A. M. Vergara, V. M. Lubecke, “Data Acquisition System for Doppler Radar Vital-Sign Monitor” IEEE EMBS, pp. 2269 – 2272, Aug 2007.

[6] O. Boric-Lubecke, V. M. Lubecke, I. Mostafanezhad, B.-K. Park, W. Massagram, B. Jokanovic, “Doppler Radar Architectures and Signal Processing for Heart Rate Extraction”, Mikrotalasna revija, pp12-17, December 2009.

[7] I. Mostafanezhad, O. Boric-Lubecke, “Benefits of Coherent Low-IF for Vital Signs Monitoring Using Doppler Radar” IEEE Trans. on Microwave Theory and Tech., Vol. 62, No. 10, pp. 2481-2487, Oct 2014.

[8] Abächerli R, Isaksen J, Schmid R, Leber R, Schmid HJ, “Digital DC-Reconstruction of AC-Coupled Electrophysiological Signals with a Single Inverting Filter”, PLoS ONE 11(3): e0150207. doi: 10.1371/journal.pone.0150207

[9] B.-K. Park, S. Yamada, O. Boric-Lubecke, and V.M. Lubecke, “Single-Channel Receiver Limitations in Doppler Radar Measurements of Periodic Motion,” IEEE Radio and Wireless Symposium, San-Diego, CA, January 2006.

[10] B. Park V. M. Lubecke, O. Boric-Lubecke, A. Høst-Madsen, “Center Tracking Quadrature Demodulation for Doppler Radar Motion Detector” IEEE MTT-S International Microwave Symposium, Honolulu, HI, USA, June 2007.

[11] M. Zakrzewski, H. Raittinen, and J. Vanhala, “Comparison of Center Estimation Algorithm for Heart and Respiration Monitoring With Microwave Doppler Radar”, IEEE Sensors Journal, Vol 12 Issue 3, pp. 627-634, March 2012

[12] I. Kasa, “A circle fitting procedure and its error analysis”, IEEE Trans. on instrumentation and measurement, Vol IM-25, Issue 1 pp. 8-14, March 1976

[13] W. Redman-White, D.M.W. Leenerts, ‘1/f noise in Passive CMOS Mixers for Low and Zero IF Integrated Receivers’

[14] M. Margraf, G. Boeck, “Analysis and Modeling in Low-Frequency Noise in Resistive FET Mixers,” IEEE Trans. on Microwave Theory and Tech., Vol. 52, No. 7, pp. 1709-1718, July2004.

[15] C.-Y. Kim, J.G. Kim, J.H. Oum, J.R. Yang, D.-K. Kim, J.H. Choi, S.-W. Kwon, S.-H. Jeon, J.-W. Park, S. Hong, “Tx Leakage Cancellers for 24 GHz and 77 GHz Vehicular

Radar Applications" Microwave Symposium Digest, 2006. IEEE MTT-S International Microwave Symposium, June 2006 Page(s): 1402 – 1405

[16] D. Nguyen, S. Yamada, B-K. Park, O. Boric-Lubecke, A. Host-Madsen, "Noise Considerations for Remote Detection of Life Signs with Microwave Doppler Radar", IEEE EMBS. Annual International Conference, August 22-26. 2007

[17] Analog Devices, "Op Amp Noise Relationships: 1/f Noise, RMS Noise, and Equivalent Noise Bandwidth", MT-048 Tutorial

[18] B. R. Mahafza, "Radar Systems Analysis And Design using MATLAB", CRC Press, ISBN 9781439884959, May 20 2013

[19] J. E. Kiriazi, O. Boric-Lubecke, V. M. Lubecke,"Dual Frequency Technique for Cardiopulmonary Effective RCS and Displacement", IEEE Sensors Journal, Vol 12 Issue 3 pp574-582, March 2012